Applied Ocean Research 62 (2017) 100–118

Contents lists available at ScienceDirect

Applied Ocean Research

journal homepage: www.elsevier.com/locate/apor

Predicting the effect of biofouling on ship resistance using CFD

Yigit Kemal Demirel*, Osman Turan, Atilla Incecik

Department of Naval Architecture, Ocean and Marine Engineering, University of Strathclyde, Henry Dyer Building, 100 Montrose Street, Glasgow, G4 0LZ, UK

ARTICLE INFO

Article history:
Received 27 June 2016
Received in revised form 1 December 2016
Accepted 6 December 2016

Keywords:
Biofouling
Ship resistance
Computational fluid dynamics
Hull roughness

ABSTRACT

This paper proposes a Computational Fluid Dynamics (CFD) based unsteady RANS model which enables the prediction of the effect of marine coatings and biofouling on ship resistance and presents CFD simulations of the roughness effects on the resistance and effective power of the full-scale 3D KRISO Container Ship (KCS) hull.

Initially, a roughness function model representing a typical coating and different fouling conditions was developed by using the roughness functions given in the literature. This model then was employed in the wall-function of the CFD software and the effects of a typical as applied coating and different fouling conditions on the frictional resistance of flat plates representing the KCS were predicted for a design speed of 24 knots and a slow steaming speed of 19 knots using the proposed CFD model. The roughness effects of such conditions on the resistance components and effective power of the full-scale 3D KCS model were then predicted at the same speeds. The resulting frictional resistance values of the present study were then compared with each other and with results obtained using the similarity law analysis. The increase in the effective power of the full-scale KCS hull was predicted to be 18.1% for a deteriorated coating or light slime whereas that due to heavy slime was predicted to be 38% at a ship speed of 24 knots. In addition, it was observed that the wave resistance and wave systems are significantly affected by the hull roughness and hence viscosity.

1. Introduction

Shipping has been, and still is, one of the most important methods of transport, with more reliance and importance now being placed on this mode of transport as a consequence of advances in shipping technology and the ability of ships to store and transport increasing capacities of goods. However, these improvements bring some problems to the industry due to an increase in fuel consumption, which is detrimental to the environment and which erodes company revenues. Although other forms of fuel power exist, such as wind energy and solar power, carbon-based fuel is currently the only way for ships to run effectively. For this reason, minimising fuel consumption is crucial for shipping companies. Such companies have therefore attempted to determine the optimum operation and maintenance approaches to either decrease the cost of operations or to increase the profit of the company. The release of harmful gases due to the use of carbon-based fuel is another reason that shipping companies should aim to reduce the fuel consumption of their ships. Some regulations, such as the Energy Efficiency Design Index (EEDI) [1] and the Ship Energy Efficiency Management Plan (SEEMP) [2], and recommended practices such as the Energy Efficiency Operational Indicator (EEOI) [3] have been implemented in recent times to limit the quantities of harmful gases that are released into the environment as a result of the fuel consumed by ships.

Although shipping is marginally more environmentally friendly than other forms of transportation, such as aviation and land, it was reported that ships released 870 million tons of CO_2 in 2007, which is equivalent to 2.7% of the total CO_2 emissions that year [4]. The International Maritime Organization (IMO) has therefore been forced, due in part to an increase in public awareness, to devise and implement energy efficiency and GHG regulations. As 95% of the world's cargo is transported by sea [5], a means of reducing the frictional resistance of ships would dramatically reduce their fuel consumption, leading to reduced carbon emissions worldwide. The best method to reduce frictional resistance is to apply a treatment to a ship's hull, to minimise its physical and biological roughness. Physical roughness can be minimised by applying some preventative measures, but biological roughness (fouling) is more difficult to control.

Marine biofouling is an increasing problem from both economic and environmental points of view in terms of increased resistance,

* Corresponding author.
E-mail address: yigit.demirel@strath.ac.uk (Y.K. Demirel).

http://dx.doi.org/10.1016/j.apor.2016.12.003

Nomenclature

k_s	Equivalent sand grain roughness height
Rt_{50}	Average hull roughness
δ	Boundary layer thickness
$u\tau$	friction velocityFriction velocity
ΔU^+	Roughness function
k^+	Roughness Reynolds number
κ	von Karman constant
y^+	Non-dimensional wall distance
B	Smooth wall log-law intercept
ρ	Density
$\bar{u}_i$	Averaged Cartesian components of the velocity vector
$\rho\overline{u'_i u'_j}$	Reynolds stresses
p	Mean pressure
$\bar{\tau}_{ij}$	Mean viscous stress tensor components
μ	Dynamic viscosity
Δt	Time step
V	Ship speed
U	Axial velocity
L	Ship length
L_{BP}	Length between the perpendiculars
L_{WL}	Length of waterline
B_{WL}	Beam at waterline
D	Depth
T	Design draft
S	Wetted surface area
∇	Displacement
C_B	Block coefficient
1 + k	Form factor
Fr	Froude number
Re	Reynolds number
R_T	Total resistance
R_F	Frictional resistance
R_R	Residuary resistance
R_W	Wave resistance
R_{VP}	Viscous pressure resistance
P_E	Effective power
C_T	Total resistance coefficient
C_F	Frictional resistance coefficient
C_R	Residuary resistance coefficient
C_W	Wave resistance coefficient
C_{VP}	Viscous pressure resistance coefficient
$C_{T,smooth}$	Total resistance coefficient in smooth condition
$C_{T,rough}$	Total resistance coefficient in rough condition
ΔC_T	Increase in total resistance coefficient due to surface roughness
ΔC_F	Added resistance coefficient due to surface roughness
ΔP_E	Increase in effective power due to surface roughness
D (%)	Relative difference
p_a	Apparent order
r, r_{21}, r_{32}	Grid refinement factors
ϕk	Key variable on the k^{th} grid
ϕ_{ext}^{21}	Extrapolated value
e_a^{21}	Napproximate relative error
e_{ext}^{21}	Extrapolated relative error
GCI_{fine}^{21}	Fine-grid convergence index

increased fuel consumption, increased GHG emissions and transportation of harmful non-indigenous species (NIS). It should be kept in mind that even a small amount of fouling may lead to a significant increase in fuel consumption. In particular, hard-shelled fouling can cause a considerable rise in ship frictional resistance, and hence a ship's fuel consumption. Hard-shelled barnacles can also deteriorate the paint and cause other problems such as corrosion. It should be noted that the impact of fouling on ship performance is greatly dependent on the type and coverage of fouling [6].

Due to its negative effects on ship efficiency and the marine environment, it is very desirable to mitigate the accumulation of biofouling on ship hulls. Marine coatings are prevalently used to smooth hull surfaces and if applied with a proper cathodic protection system also prevents corrosion [7]. An ideal marine coating should be smooth enough to improve the surface properties of a hull in the as applied condition and should be effective against marine biofouling which occurs over time.

While improving the energy efficiency of existing ships retrofitted with new antifouling (AF) paints, it is equally important to accurately model the potential effects of biofouling on ship resistance and to demonstrate the importance of the mitigation of such effects by carrying out scientific research. However, at present, there is no complete method available to predict the effect of biofouling on ship frictional resistance. The ITTC [8] therefore recommends researchers to develop new formulae or methods, using experimental data, for the prediction of the effects of coatings and biofouling on ship resistance

Granville [9,10] proposed a similarity law scaling procedure for the prediction of the effects of a particular roughness on the frictional resistance of any arbitrary body covered with the same roughness, utilising the experimentally obtained roughness functions of such surfaces. The only real assumption of the method is that the outer layer similarity holds in the mean velocity profiles for smooth and rough-wall boundary layers. That is to say, the velocity-defect profiles collapse to a single curve in the outer layer. Some examples of the use of this method are given by Loeb et al. [11], Haslbeck and Bohlander [12], Schultz [6,13–15], Shapiro [16], Flack and Schultz [17] and Schultz, Bendick [18]. Recently, Walker et al. [19] conducted experiments using both antifouling and fouling-release hull coatings and scaled up the results to predict the effects of these coatings on a mid-sized naval ship. Grigson [20] proposed a method which is partly experimental and partly theoretical, just like the ones proposed by Granville [9,10]. Some numerical methods were also proposed for general rough surfaces rather than hull roughness, such as Christoph and Pletcher [21], Lakehal [22] and Greígoire et al. [23].

When it comes to CFD-based models, there are fewer studies investigating the roughness effects of coatings and biofouling on ship resistance. Patel [24] mentioned that the most complex problems for CFD are full scale Reynolds number flows and simulating surface roughness. Currently, physical modelling of the roughness sources, such as coatings or biofouling, in CFD is practically impossible due to their complex geometries. However, once the relation of $\Delta U^+ = f(k^+)$ is known, it can be employed in the wall-function or the turbulence models of the CFD software, as discussed by Patel [24]. The use of CFD-based unsteady RANS models is of vital importance, since the phenomenon can be simulated by means of a fully non-linear method. For instance, one particular roughness Reynolds number value, k^+, and roughness function value, ΔU^+, are taken into consideration when a prediction is made for a specific condition in the similarity law scaling procedure of Granville [9]. However, the k^+ vs. ΔU^+ value is not uniform even on a flat plate due to differences in the friction velocity, $u\tau$, distribution. That is to say, $u\tau$ varies along the flat plate. This effect, however, can be simulated using CFD-based models as $u\tau$ is dynamically computed for each discretised cell. Therefore, the resulting frictional resistance can be more accurately computed using CFD methods.

Several studies exist which model the effects of a uniform sand-grain roughness, though not necessarily the hull roughness,

either using wall-functions (e.g. Suga et al. [25], Apsley [26]) or using near-wall resolution (e.g. Krogstad [27], Aupoix [28]). Eça and Hoekstra [29] showed that the effect of uniform sand-grain roughness on the frictional resistance of flat plates of full-scale ship lengths at full-scale ship speeds can be accurately simulated using either wall-functions or near-wall resolution. Date and Turnock [30] demonstrated the required techniques to predict the skin friction of flat plates using RANS solvers and also showed that the effect of surface roughness on skin friction can be predicted using CFD software. They modified the wall-functions of a piece of commercial CFD software by modifying the wall function-coefficient (log-layer constant). Nevertheless, this method does not directly reflect the roughness effect on the frictional resistance and does not compute these effects dynamically. Leer-Andersen and Larsson [31], on the other hand, employed roughness functions in a commercial CFD code and predicted the skin friction of full scale ships. However, they used a specific module of the software, which incorporates thin boundary layer methods with a potential flow solver, and the study does not include unsteady RANS calculations. Izaguirre-Alza et al. [32] used the CFD software package STAR-CCM+ to simulate their experiments and validate the roughness feature of the software. Although the comparison shows a very good agreement between the experimental data and the evaluated results, there is no evidence of the use of a specific roughness function model, rather than the built-in roughness function. Khor and Xiao [33] investigated the effects of fouling and two antifouling coatings on the drag of a foil and a submarine by employing a CFD method. They used the equivalent sand grain roughness height and the built-in wall-function which considers the uniform sand-grain roughness function model proposed by Cebeci and Bradshaw [34], based on Nikuradse's data [35]. Currently, the ITTC [36] is still questioning the validity of the roughness model and equivalent sand grain roughness used in CFD applications for hull roughness, since it is known that the built-in roughness function model is based on uniform, closely packed sand roughness, whereas the roughness functions of real engineering surfaces do not show this behaviour. Castro, Carrica [37] carried out unsteady RANS CFD simulations of a full-scale KCS model with hull coating roughness using wall-functions. However, they used a constant roughness function and the roughness allowance formulation proposed by the ITTC [38]. They did not attempt to employ a new type of roughness function model which is more appropriate for real engineering surfaces, especially for fouled surfaces. Recently, Demirel et al. [39] proposed a CFD model for the frictional resistance prediction of antifouling coatings. Haase et al. [40] showed the applicability of the CFD approach to predict the sand grain roughness effects on the frictional resistance of flat plates as well as on the resistance of catamarans.

As discussed above, current numerical methods for the prediction of the effect of biofouling on frictional resistance are limited by the use of boundary layer similarity law analysis. This method can only calculate the effect of a given surface roughness on the frictional resistance of a flat plate of ship length. Although this can be seen as a reasonable assumption, since the surface roughness is not expected to significantly affect the pressure drag, it is still worth investigating the phenomenon by means of a fully nonlinear method, such as CFD, to investigate the roughness effect of biofouling on the resistance components of a ship in detail. In addition, a typical CFD work could take the effect of spatial distribution of fouling on the total drag of the hull into consideration.

To the best of this author's knowledge, no specific CFD model exists to predict the roughness effect of biofouling on ship resistance. The aim of the present paper is therefore to fill this gap by employing a modified wall-function in the CFD software package and to investigate the roughness effect of biofouling on the resistance components. The proposed approach enables the prediction of the resistance coefficients of full-scale 3D ship hulls bearing a typical coating and a range of fouling conditions.

The main advantage of the proposed model is that it enables the use of a simple roughness length scale to predict the effect of biofouling on frictional resistance of a flat plate of ship length, similar to that of Demirel et al. [39] as well as on the resistance components and effective power of a full-scale ship.

In this study, the experimental data of Schultz and Flack [41] were used to establish a suitable roughness function model for different fouling conditions. Corresponding roughness heights of Schultz [6] representing different fouling conditions were used to model the different surfaces. This roughness function model was then employed in the wall-function of the CFD software package STAR-CCM+.

Following this, a typical case study was performed through CFD simulations of towing tests involving a flat plate of length 232.5 m, representing the Kriso Container Ship (KCS), with different surface conditions at different service speeds. Frictional resistance coefficients were computed and the increases in the frictional resistance of the flat plate representing KCS due to such fouling conditions were predicted.

Unsteady RANS CFD simulations of the roughness effects of marine coatings and biofouling on the full-scale 3D KCS were then performed using the same CFD model. A full-scale 3D KCS hull appended with a rudder was used due to the existence of available experimental data for comparison purposes, and in order to enable a reasonable comparison. The model was first towed in smooth conditions at a design speed of 24 knots and the resulting total resistance coefficient was compared and validated with the total resistance coefficient extrapolated using the experimental data. Following this, typical parametric case studies were performed at a design speed of 24 knots and a slow steaming speed of 19 knots. These involved changing the surface conditions by employing the roughness function model and corresponding roughness length scales proposed, to represent a typical coating and a range of fouling conditions, while holding the other parameters constant. Frictional, residuary and total resistance coefficients of the KCS were directly computed whereas the wave resistance coefficients were calculated using the form factor of the KCS. The effect of hull roughness on the wave systems were also investigated. Moreover, the increases in the effective power of the KCS due to such surface conditions were predicted using the present results.

The present results, obtained using flat-plate CFD simulations and using full-scale 3D KCS model were compared with each other and with those obtained using the similarity law analysis of Granville [3].

This paper is organised as follows: The roughness functions used to represent a range of biofouling conditions are presented in Section 2, while a new wall-function formulation is proposed and details of the numerical setup are covered in Section 3. In Section 4, the CFD results obtained using flat-plate and full-scale 3D approach were presented together with the results obtained using the similarity law analysis. Finally, the results of the study are discussed in Section 5, along with recommendations for future avenues of research.

2. Roughness functions

The velocity profile in the log-law region of the turbulent boundary layer can be defined by

$$U^+ = \frac{1}{\kappa}\ln(y^+) + B - \Delta U^+ \tag{1}$$

in which κ is the von Karman constant, y^+ is the non-dimensional normal distance from the boundary, B is the smooth wall log-law intercept and ΔU^+ is the roughness function. By using Eq. (1), one

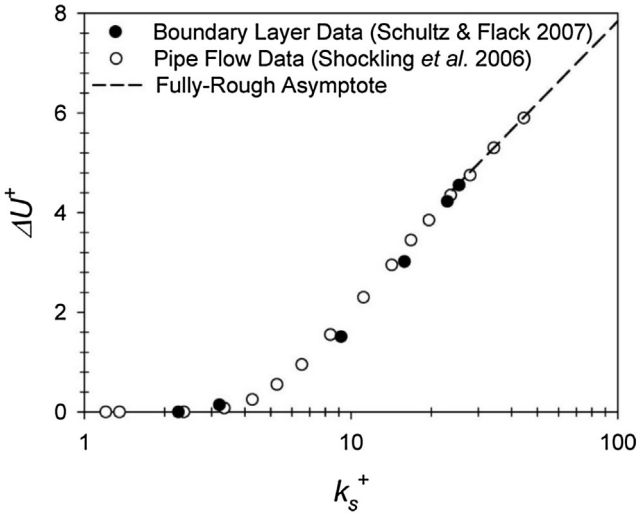

Fig. 1. Roughness function vs. roughness Reynolds numbers [6].

can represent the change in the velocity profile due to roughness using ΔU^+, and the velocity profile can be defined by simply subtracting ΔU^+ from the smooth velocity profile. It should be borne in mind that ΔU^+ simply vanishes in the case of a smooth condition. ΔU^+ values are typically obtained experimentally, since there is no universal roughness function model for every kind of roughness. Reference may be made to Jiménez [42] for a comprehensive review on rough wall turbulent boundary layers.

Schultz and Flack [41] determined the roughness functions for three dimensional rough surfaces similar to those used by Shockling et al. [43]. Schultz [6] proposed that the roughness function behaviour of a range of fouling conditions follow the roughness functions of Schultz and Flack [41] and Shockling et al. [43], based on his previous work presented in Schultz [15]. This is a reasonable assumption, since the roughness functions of real surfaces are expected to show behaviour that is between the monotonic Colebrook and inflectional Nikuradse type roughness functions, such as those presented by Schultz and Flack [41] and Shockling et al. [43], as shown in Fig. 1. In addition, Schultz [6] presented the equivalent sand roughness heights for a range of coating and fouling conditions together with the NSTM (Naval Ships' Technical Manual) [44] rating and average coating roughness (Rt_{50}) based on his extensive experiments including Schultz [15] (Table 1).

In this paper's study, the roughness function values of Schultz and Flack [41] shown in Fig. 1 were used to develop a roughness function model to be employed in the CFD software to represent the coating and fouling conditions given by Schultz [6], as shown in Table 1.

The present predictions were made based on the assumptions that the given fouling conditions can be represented by these roughness functions and roughness length scales. Schultz [6] validated these assumptions and this method by comparing his results with other studies such as Hundley and Tate [45] and Haslbeck and Bohlander [12], documenting the effects of coatings and biofouling on ship powering through full-scale trials.

An appropriate roughness function model was fitted to the roughness function values of Schultz and Flack [41], given in Eq. (5). This roughness function model is presented such that it is in the form of the built-in roughness function model of STAR-CCM+ for application convenience.

Table 1
A range of representative coating and fouling conditions [6].

Description of condition	NSTM rating[a]	k_s (μm)	Rt_{50} (μm)
Hydraulically smooth surface	0	0	0
Typical as applied AF coating	0	30	150
Deteriorated coating or light slime	10–20	100	300
Heavy slime	30	300	600
Small calcareous fouling or weed	40–60	1000	1000
Medium calcareous fouling	70–80	3000	3000
Heavy calcareous fouling	90–100	10000	10000

[a] NSTM [44].

3. Numerical modelling

3.1. Mathematical formulation

An Unsteady Reynolds-Averaged Navier-Stokes (URANS) method was used to solve the governing equations in this study. These mass and momentum conservation equations were solved by the commercial CFD software STAR-CCM+. The averaged continuity and momentum equations for incompressible flows are given in tensor notation and Cartesian coordinates by Eqs. (2) and (3)

$$\frac{\partial(\rho\bar{u}_i)}{\partial x_i} = 0, \tag{2}$$

$$\frac{\partial(\rho\bar{u}_i)}{\partial t} + \frac{\partial}{\partial x_j}\left(\rho\bar{u}_i\bar{u}_j + \rho\overline{u'_i u'_j}\right) = -\frac{\partial\bar{p}}{\partial x_i} + \frac{\partial\bar{\tau}_{ij}}{\partial x_j} \tag{3}$$

where ρ is density, $\bar{u}_i$ is the averaged Cartesian components of the velocity vector, $\rho\overline{u'_i u'_j}$ is the Reynolds stresses and p is the mean pressure. $\bar{\tau}_{ij}$ are the mean viscous stress tensor components, as shown in Eq. (4)

$$\bar{\tau}_{ij} = \mu\left(\frac{\partial\bar{u}_i}{\partial x_j} + \frac{\partial\bar{u}_j}{\partial x_i}\right) \tag{4}$$

in which μ is the dynamic viscosity.

The solver uses a finite volume method which discretises the governing equations. A second order convection scheme was used for the momentum equations and a first order temporal discretisation was used. The flow equations were solved in a segregated manner. The continuity and momentum equations were linked with a predictor-corrector approach.

The SST (Shear Stress Transport) k-ω turbulence model was used in order to complete the RANS equations, which blends the k-ω model near the wall and the k-ε model in the far field. For the flat-plate simulations, the Courant-Frederich-Lewis (CFL) number was always held at values less than unity to ensure the numerical stability. It is of note that the ITTC [36] recommend the use of $\Delta t = 0.005 \sim 0.01$ L/V, where L is ship length and V is ship speed, for the selection of the time step. However, the time step size of the simulations of the KCS hull was set to $\sim 0.0005 L_{BP}/V$, which is ten times lower than the recommendation of the ITTC [36], to ensure a reliable solution for such a complex phenomenon. It should be noted that the full-scale ship model was kept fixed, i.e. it was not free to sink and trim, throughout all simulations.

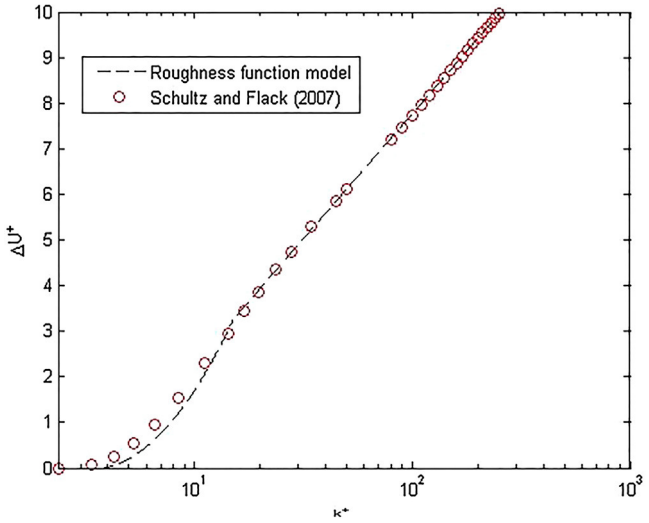

Fig. 2. The proposed CFD roughness function model together with the roughness functions.

3.2. Proposed wall-function approach for fouling conditions

An appropriate roughness function model for a range of representative coating and fouling conditions for use in STAR-CCM+ is proposed by Eq. (5).

$$\Delta U^+ = \begin{cases} 0 \rightarrow k^+ < 3 \\ \frac{1}{\kappa}\ln\left(0.26k^+\right)^{\sin\left[\frac{\pi}{2}\frac{\log(k^+/3)}{\log(5)}\right]} \rightarrow 3 < k^+ < 15 \\ \frac{1}{\kappa}\ln\left(0.26k^+\right) \rightarrow 15 < k^+ \end{cases} \quad (5)$$

Shown for comparison in Fig. 2 is the proposed roughness function model given by (5) and roughness functions of Schultz and Flack [41].

The proposed model for a range of representative coating and biofouling conditions in this paper is in a similar form to the built-in wall function of STAR-CCM+ in terms of flow regimes. That is to say, the proposed roughness function model and the wall-law have 3 flow regimes, namely a hydraulically smooth regime, a transitionally rough regime and a fully rough regime, which are similar to those proposed by Cebeci and Bradshaw [34] based on Nikuradse's data [35]. It is evident from Fig. 2 that an excellent agreement is achieved in the fully rough regime while a reasonable match is obtained in the transitionally rough regime. General information about the wall-function approach and details of the application of roughness functions through wall-functions can be found in [39].

3.3. Geometry and boundary conditions

The geometry of the plate representing the KCS is shown in Fig. 3. The boundary conditions of the simulations were chosen to represent the plate being completely submerged in an infinite ocean, with similarity to the full scale prediction simulations presented in [39]. The boundary conditions and the positioning of the boundaries were therefore chosen to be similar to those given in [39], as shown in Fig. 4.

The KRISO Container Ship (KCS) appended with a rudder was used in this paper's full-scale 3D simulations since experimental data for this hull is publicly available and a large body of related CFD studies exist in the literature (e.g. Larsson et al. [46], Zhang [47], Castro et al. [37], Carrica et al. [48] and Tezdogan et al. [49]).

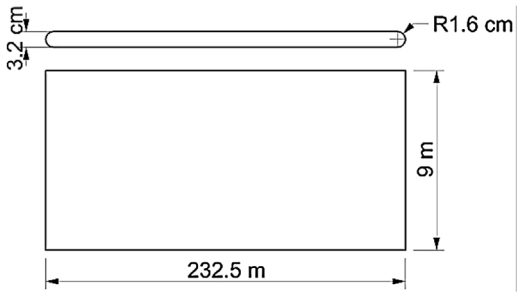

Fig. 3. The plates representing the KCS.

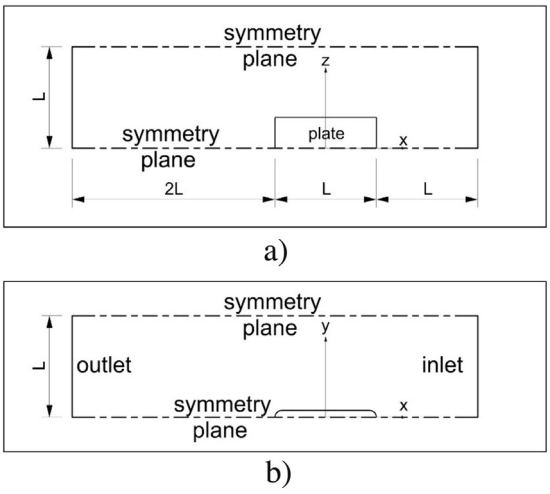

Fig. 4. a) profile view of the domain and b) top view of the domain, showing the dimensions and boundary conditions [39].

Table 2
Principal particulars of the KCS, adapted from Tezdogan et al. [49] and Kim et al. [50].

Length between the perpendiculars (L_{BP})	230.0 m
Length of waterline (L_{WL})	232.5 m
Beam at waterline (B_{WL})	32.2 m
Depth (D)	19.0 m
Design draft (T)	10.8 m
Wetted surface area	9498 m^2
Displacement (∇)	52030 m^3
Block coefficient (C_B)	0.6505
Design Speed	24 knots
Froude number (Fr)	0.26

Additionally, the KCS has a very similar shape to commercial container ships, meaning the results will give an indication of how fouling effects the performance of real commercial container ships.

The principal particulars, body plans and side profiles of the full-scale KCS model are given in Table 2 (adapted from Tezdogan et al. [49] and Kim et al. [50]), and Fig. 5 [50], respectively.

The boundary conditions of the simulations were chosen to represent the full-scale KCS model being towed in a deep water condition. Fig. 6 depicts an overview of the domain with the KCS model and the selected boundary conditions.

The two opposite faces at the x-direction of the domain, i.e. the left-hand face (positive x-direction) and right-hand face (negative x-direction) of the domain in the top view were modelled as a velocity inlet and a pressure outlet, respectively. A symmetry plane was used to halve the required cell numbers and to reduce the computational demand since this does not significantly affect the computations. A velocity inlet boundary condition was set to the top, bottom and side (the negative y-direction) boundaries. It

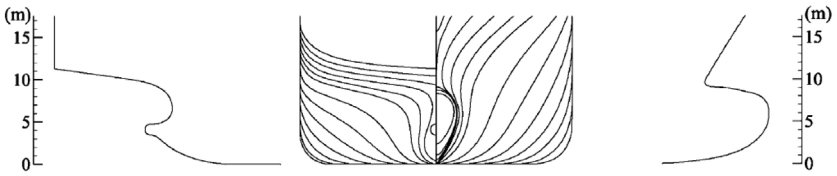

Fig. 5. Body plan and side profiles of the KCS model [50].

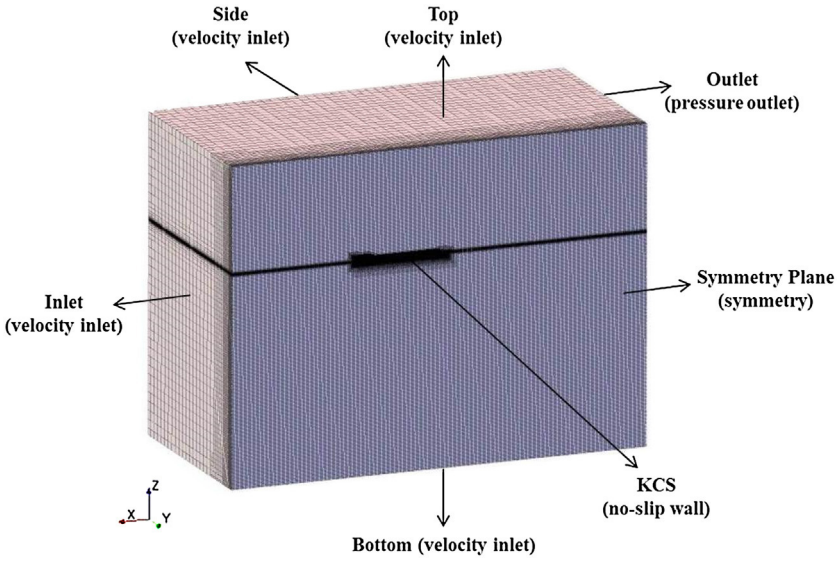

Fig. 6. An overview of the domain with the selected boundary conditions.

should be kept in mind that the initial flow velocity at all inlet conditions was set to the velocity of the flat wave, i.e. a ship speed of 24 knots, in the negative x-direction. The selection of the velocity inlet for the top and side of the domain therefore enables the flow at the top and side of the domain to be parallel to the outlet boundary, which prevents reflections from these boundaries. In addition, the representation of the deep water and infinite air conditions was facilitated by the use of a velocity inlet boundary condition for the top and bottom boundaries. The KCS hull itself has a no-slip rough wall condition to represent the roughness on the hull.

Another critical selection is the positioning of the boundaries, especially the downstream outlet boundary and the upstream inlet boundary. The inlet is placed at $\sim 1.5L_{BP}$ lengths upstream and the outlet boundary is placed at $\sim 2.5L_{BP}$ lengths downstream, to ensure boundary independent solutions are produced. Similarly, the top is located at $\sim 1.5L_{BP}$ and the bottom and the side are positioned at $\sim 2.5L_{BP}$ away from the KCS hull. It is of note that the selection of these boundary conditions and the positioning of the boundaries were made based on the recommendations and applications reported in CD-ADAPCO [51]. The locations of the boundaries are shown in Fig. 7.

It should be noted that the VOF wave damping capability of the software was applied to the outlet and all velocity inlet boundaries, namely the inlet, bottom, top and side, with a damping length equal to $\sim 1L_{BP}$, to prevent reflections from these boundaries.

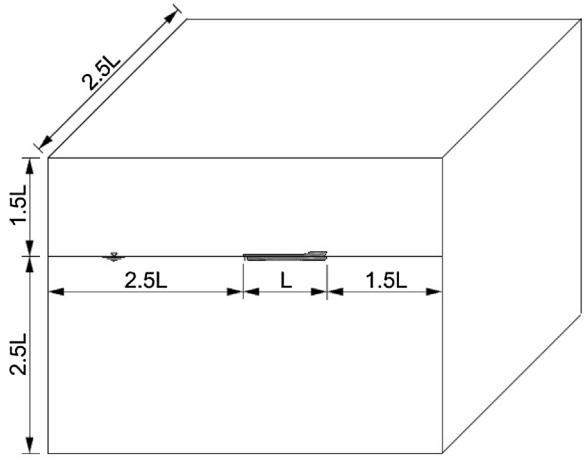

Fig. 7. The positions of the boundaries. (L: length of the ship between perpendiculars).

3.4. Mesh generation

A cut-cell grid with prism layer mesh on the walls was generated using the automatic mesh generator in STAR-CCM+. Additional refinements were applied to give finer grids in the critical regions, such as the area immediately around the plate, the areas around the trailing and leading edges, and the top edge of the plate as well as the area immediately around the hull and rudder, the area where the bow encounters the free surface, the area where water breaks with the hull stern, and the area in the wake generated by the ship. The mesh generation was achieved using similar techniques to those explained in [39]. Also, convergence tests were performed to ensure grid-independent mesh configurations, as well as to predict the uncertainty of the CFD simulations.

A special near-wall mesh resolution was applied to all surfaces with no-slip boundary conditions based on the roughness height values corresponding to each fouling condition. For this reason, the near-wall cell numbers varied for some of the fouling conditions. These differences resulted in different total cell numbers. The numbers of the total cells generated are given in Table 3 for flat plate and

Table 3
Total cell numbers for flat plate.

Surface Condition (k_s [μm])	Cell numbers
$k_s = 0$, $k_s = 30$, $k_s = 100$, $k_s = 300$	5.5×10^6
$k_s = 1000$	5.28×10^6
$k_s = 3000$	4.5×10^6
$k_s = 10000$	4×10^6

Table 4
Total cell numbers for the full-scale KCS hull.

Surface Condition (k_s [μm])	Cell numbers
$k_s = 0$, $k_s = 30$, $k_s = 100$, $k_s = 300$	4.09×10^6
$k_s = 1000$	4.00×10^6
$k_s = 3000$	3.70×10^6
$k_s = 10000$	3.58×10^6

in Table 4 for the full-scale simulations of the KCS hull. Near-wall mesh generation must be performed with care since this is directly related to the hull roughness due to marine coatings and biofouling. The prism layer thickness and prism layer numbers were, therefore, determined such that y^+ is always higher than 30, and higher than k^+, as per CD-ADAPCO [51]'s suggestion.

Fig. 8 shows cross-sections of the meshed domain whereas Fig. 9 shows the volume mesh on the KCS hull and rudder. It is of note that, from this point onward, the figures show the whole sections as if there is no symmetrical boundary, owing to the visual transform feature of the software.

Fig. 8 demonstrates the cross-section from the centreline of the hull and the free surface and shows only a portion of the cross-sections for visual convenience, since the domain is rather large. The refinements to capture the free surface and Kelvin wake are clearly visible in Fig. 8.

Fig. 9 clearly shows the effects of additional refinements on the KCS hull and rudder, especially the ones applied to the free surface, bow and stern regions.

Table 5
C_F results at different mesh configurations for the flat-plate KCS case.

Mesh configuration	Total No. of Cells	C_F (CFD)
Coarse	2.2×10^6	0.0020086
Medium	3.3×10^6	0.0020145
Fine	5.5×10^6	0.0020222

4. Results

4.1. Grid sensitivity study

Systematic studies were performed using the flat plates covered with heavy slime and using the KCS hull appended with a rudder with a smooth surface condition, in order to carry out a grid sensitivity study and to predict the CFD uncertainties. In order to observe the effect of cell numbers on the key variable, (C_F in flat-plate case and C_T in full-scale KCS hull case), the domain was discretised in three different resolutions and the simulations were run for each configuration. The grid refinement factor, r, was chosen to be $\sqrt{2}$ as used by Tezdogan et al. [49].

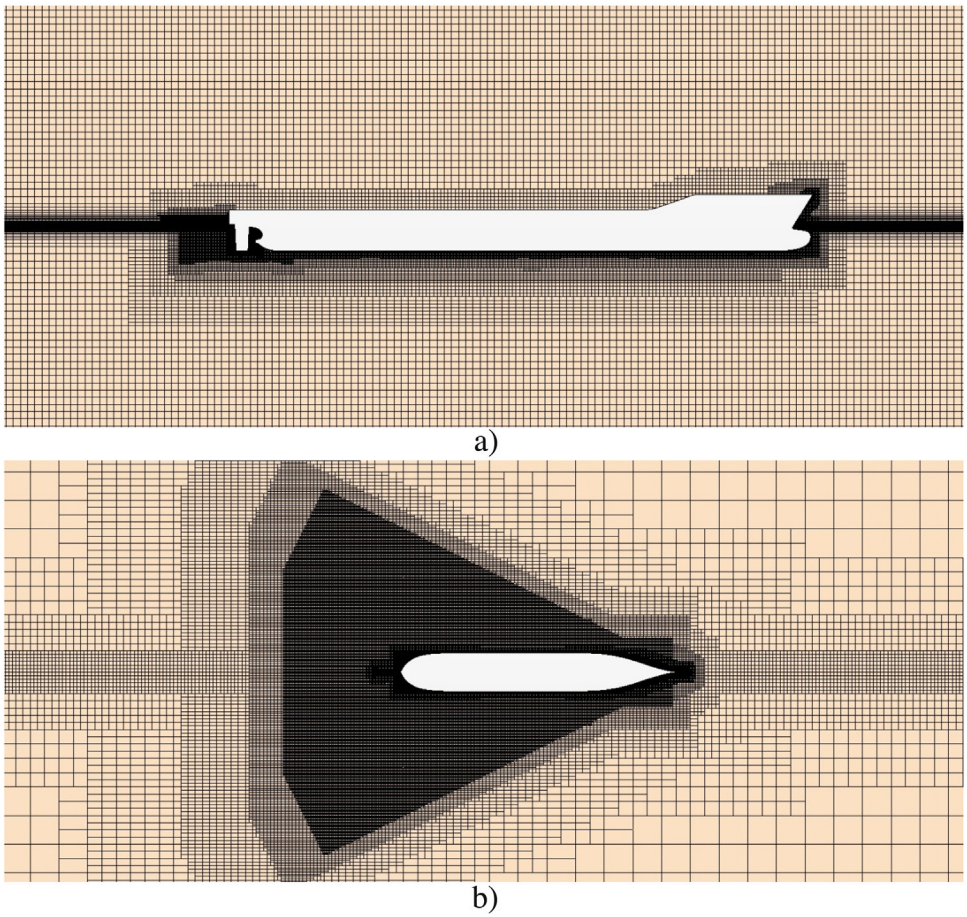

Fig. 8. a) Profile view cross-section b) top view cross-section of the domain.

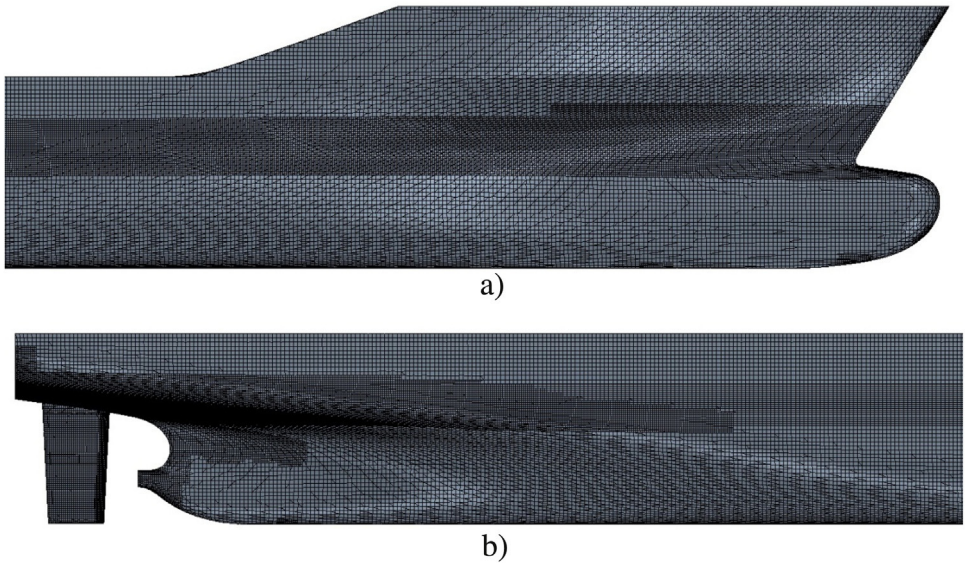

Fig. 9. Volume meshes on the a) bow, b) stern of the KCS hull and rudder.

Table 6
C_T results at different mesh configurations for the full-scale KCS at 24 knots (Relative Difference, D (%), is based on the C_T value extrapolated using the experimental data of Kim et al. [50]).

Mesh configuration	Total No. of Cells	C_T (CFD)	D (%)
Coarse	1.07×10^6	0.002120	2.30
Medium	2.04×10^6	0.002113	1.94
Fine	4.09×10^6	0.002097	1.17

The frictional resistance coefficients for each mesh configuration were computed and are given in Table 5 for the flat-plate KCS case.

Similarly, the total resistance coefficients for each mesh configuration were computed at a design speed of 24 knots and are given in

Table 6 for full-scale simulation of KCS hull.

From Tables 5 and 6 it is evident that the variation in drag with a $\sqrt{2}$ refinement ratio are below ~0.8% and that the total resistance coefficient was over-predicted by 1.17%.Therefore, the fine mesh configuration was selected in all subsequent computations.

4.2. Verification study

A verification study should be carried out to show the capability of the proposed model and the software for particular calculations. The Grid Convergence Index (GCI) Method based on Richardson extrapolation [52,53] was used in this paper's work for discretisation error estimation as described by Celik, Ghia [54].

The apparent order of the method, p_a, is calculated by

$$p_a = \frac{1}{\ln(r_{21})} |\ln|\varepsilon_{32}/\varepsilon_{21}| + q(p_a)| \tag{6}$$

$$q(p_a) = \ln\left(\frac{r_{21}^{p_a} - s}{r_{32}^{p_a} - s}\right) \tag{7}$$

$$s = 1 \cdot sign\left(\varepsilon_{32}/\varepsilon_{21}\right) \tag{8}$$

where r_{21} and r_{32} are refinement factors, i.e. $\sqrt{2}$ in this study, and $\varepsilon_{32} = \phi_3 - \phi_2$, $\varepsilon_{21} = \phi_2 - \phi_1$, ϕ_k is the key variable, i.e. C_F and C_T in this case, on the k^{th} grid.

The extrapolated values are obtained by

$$\phi_{ext}^{21} = \left(r_{21}^p \phi_1 - \phi_2\right) / \left(r_{21}^p - 1\right) \tag{9}$$

Table 7
Calculation of the discretisation error for C_F values of the flat plate.

	C_F
r_{21}, r_{32}	$\sqrt{2}$
ϕ_1	0.0020222
ϕ_2	0.0020145
ϕ_3	0.0020086
p_a	0.76829
${\phi ext}^{21}$	0.0020474
${e_a}^{21}$	0.38077%
${e_{ext}}^{21}$	1.2327%
${GCI_{fine}}^{21}$	1.5601%

Table 8
Calculation of the discretisation error for C_T values of the full-scale KCS.

	C_T
r_{21}, r_{32}	$\sqrt{2}$
ϕ_1	0.002097
ϕ_2	0.002113
ϕ_3	0.002120
p_a	2.3853
${\phi ext}^{21}$	0.0020846
${e_a}^{21}$	0.76299%
${e_{ext}}^{21}$	0.59698%
${GCI_{fine}}^{21}$	0.7418%

The approximate and extrapolated relative errors are calculated using the following equations, respectively.

$$e_a^{21} = \left|\frac{\phi_1 - \phi_2}{\phi_1}\right| \tag{10}$$

$$e_{ext}^{21} = \left|\frac{\phi_{ext}^{12} - \phi_1}{\phi_{ext}^{12}}\right| \tag{11}$$

The fine-grid convergence index is calculated by

$$GCI_{fine}^{21} = \frac{1.25 e_a^{21}}{r_{21}^p - 1} \tag{12}$$

The required parameters were calculated for C_F and C_T values and are presented in Table 7 for the flat plate and in Table 8 for the full-scale KCS.

As can be seen from Tables 7 and 8, numerical uncertainties of 1.56%, 0.74% were calculated for the computed C_F and C_T values respectively.

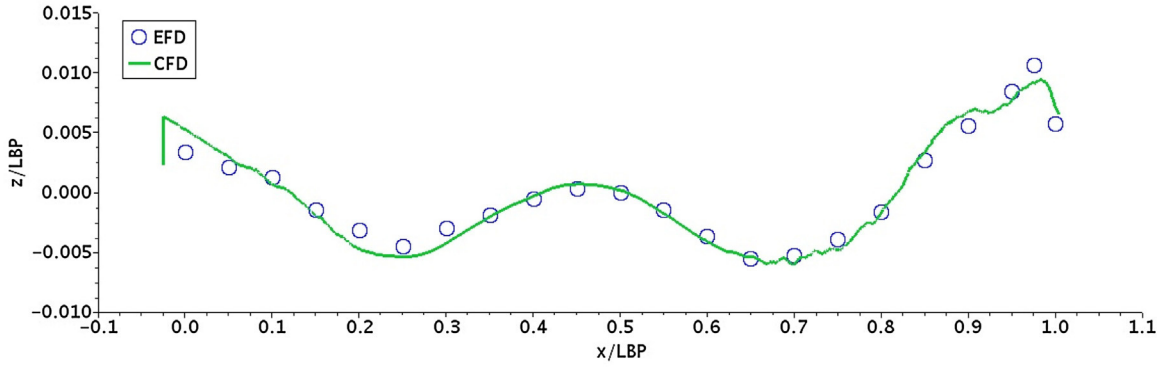

Fig. 10. Wave profile along KCS at 24 knots.

4.3. Validation study

The available experimental data for the KCS was used to validate the CFD approach using the smooth condition. During the towing tank tests conducted by Kim et al. [50], the residuary resistance coefficient for a 1/31.6 scale model of the KCS was found to be 7.250×10^{-4}, at the corresponding model speed for the full-scale speed of 24 knots (Fr = 0.26). Given that the residuary resistance is a function of Froude number, the residuary resistance coefficient of the full-scale KCS model is assumed to be the same ($C_R = 7.250 \times 10^{-4}$) and the full-scale frictional resistance coefficient, C_F, is calculated to be 1.347×10^{-3}, using the "ITTC 1957 model-ship correlation line" at the corresponding Reynolds number. The total resistance coefficient of the full-scale KCS model is therefore predicted to be 2.0725×10^{-3}. It is of note that form factor, (1 + k), was not taken into account while extrapolating.

Table 6 demonstrates the total resistance coefficients computed by CFD and extrapolated using the experimental data of Kim et al. [50], at a ship speed of 24 knots. As can be seen from Table 6, the computed total resistance coefficient, C_T, is in excellent agreement with this extrapolated data, with a difference of only ~1.17%. This CFD approach can therefore be claimed to be validated and can be used for further investigations. This model was therefore used throughout all the cases.

Shown for comparison in Fig. 10 is the computed wave profile along the hull surface of the KCS together with the wave profile measured during the towing tank tests conducted by Kim et al. [50]. Fig. 16 shows the global wave pattern around the hull surface of the KCS whereas Fig. 17 shows the wave profile along a line with constant y = 0.1509. The Kelvin wake generated by the ship is clearly visible in Fig. 16.

It is evident from Figs. 10, 16 (smooth condition) and Fig. 17 (smooth condition) that a very good agreement is achieved between the current CFD model and the experimental data of Kim et al. [50], as well as the other CFD simulations performed by other researchers (e.g. Carrica et al. [55] and Castro et al. [37]).

4.4. Effects of hull roughness

Before investigating the effects of hull roughness on the resistance components of a ship, it would be timely to describe these components in detail. The total resistance (drag) of a ship, R_T, is mainly composed of two components; the frictional resistance, R_F, and the residuary resistance, R_R, as given by (13).

$$R_T = R_F + R_R \tag{13}$$

The frictional resistance arises due to shear stresses on the hull surface while the residuary resistance is the pressure related drag which consists of the wave resistance, R_W, and viscous pressure resistance, R_{VP}, of the ship. This relation can be shown in a more explicit way by (14),

$$R_T = R_F + R_{VP} + R_W \tag{14}$$

where it is assumed $R_{VP} = kR_F$. Eq. (14) can be defined as follows:

$$R_T = R_F + kR_F + R_W = (1 + k)R_F + R_W \tag{15}$$

If these resistance components are non-dimensionalised by dividing each term by the dynamic pressure and wetted surface area of the ship hull, the resistance coefficients can be defined as follows:

$$C_T = C_F + C_R \tag{16}$$

$$C_T = C_F + C_{VP} + C_W \tag{17}$$

$$C_T = (1 + k)C_F + C_W \tag{18}$$

where C_T is the total resistance coefficient, C_F is the frictional resistance coefficient, C_R is the residuary resistance coefficient, C_{VP} viscous pressure resistance coefficient, C_W is the wave resistance coefficient.

Table 9
Comparison of the computed C_F values using different methods at full scale at 24 knots ($Re = 2.89 \times 10^9$) (Relative Difference, D (%) is based on Granville method).

SurfaceCondition (k_s [μm])	$C_F \times 10^3$				
	CFD-KCS hull		Granville	CFD-Flat plate	
	Result	D (%)		Result	D (%)
0	1.421	**5.52**	1.347	1.351	**0.3**
30	1.577	**7.32**	1.469	1.496	**1.84**
100	1.840	**5.01**	1.752	1.750	**−0.11**
300	2.120	**3.62**	2.046	2.022	**−1.17**
1000	2.514	**2.41**	2.455	2.401	**−2.20**
3000	3.014	**2.49**	2.941	2.886	**−1.87**
10000	3.741	**2.47**	3.651	3.571	**−2.20**

4.4.1. Frictional resistance

Having performed prediction studies using both flat plates representing the KCS and the full-scale KCS model itself, it would be interesting to also compare these different methods. Therefore, the following section aims to compare and discuss the results obtained using the different techniques. These techniques are full-scale 3D CFD simulations of the KCS hull (referred to as 'CFD-KCS hull'), flat plate CFD simulations (referred to as 'CFD-Flat plate') and the similarity law scaling procedure of Granville [9] (referred to as 'Granville').

Tables 9 and 10 show the frictional resistance coefficients of the KCS obtained for 7 different surface conditions, at ship speeds of 24 knots and 19 knots, using the different methods explained above. Also, the relative comparison differences which are based on the

Table 10
Comparison of the computed C_F values using different methods at full scale at 19 knots ($Re = 2.29 \times 10^9$) (Relative Difference, D (%) is based on Granville method).

Surface condition (k_s [μm])	$C_F \times 10^3$				
	CFD-KCS hull		Granville	CFD-Flat plate	
	Result	D (%)		Result	D (%)
0	1.452	**4.82**	1.385	1.386	**0.07**
30	1.559	**5.86**	1.473	1.485	**0.81**
100	1.834	**4.57**	1.754	1.750	**−0.23**
300	2.115	**3.30**	2.047	2.022	**−1.22**
1000	2.509	**2.10**	2.457	2.401	**−2.28**
3000	3.006	**2.11**	2.944	2.886	**−1.97**
10000	3.733	**2.14**	3.655	3.578	**−2.10**

results obtained using Granville method are listed in the tables. Since the experimental C_F values are not available, only the results from CFD and the similarity law analysis are given for the frictional drag coefficients in the table.

As Table 9 and 10 jointly show, the results obtained using both of the present CFD methods used in this paper agreed with the results obtained using Granville's method, with differences of less than ∼7%. This indicates that the present CFD model stands as a suitable technique with which to predict roughness effects on the frictional resistance of flat plates of model-scale and full-scale ship lengths, and of full-scale 3D ship hulls. The physical adequacy of the CFD approach was therefore demonstrated. The results and comparisons of Haase et al. [40] also support the applicability of the general CFD approach to accurately account for the roughness effects on the frictional resistance of flat plates and ships.

It is interesting to note that the all C_F values obtained at ship speeds of 24 knots and 19 knots using "CFD-KCS hull" method are higher than those obtained using "CFD-Flat plate" method and those obtained using "Granville" method.

The increase in the frictional resistance of the KCS due to different surface conditions with respect to those of a hydraulically smooth, predicted using the different techniques, are demonstrated in Table 11 and Fig. 11 for 24 knots and in Table 12 and Fig. 12 for 19 knots.

Table 11
Comparison of the computed% ΔC_F values using different methods at full scale at 24 knots ($Re = 2.89 \times 10^9$).

Description of condition	% ΔC_F		
	CFD-KCS hull	CFD-Flat plate	Granville
Hydraulically smooth surface	–	–	–
Typical as applied AF coating	10.9	10.7	9
Deteriorated coating or light slime	29.4	29.5	30
Heavy slime	49.2	49.7	51.8
Small calcareous fouling or weed	76.9	77.7	82.2
Medium calcareous fouling	112.1	113.6	118.3
Heavy calcareous fouling	163.2	164.3	171.0

Table 12
Comparison of the computed% ΔC_F values using different methods at full scale at 19 knots ($Re = 2.29 \times 10^9$).

Description of condition	% ΔC_F		
	CFD-KCS hull	CFD-Flat plate	Granville
Hydraulically smooth surface	–	–	–
Typical as applied AF coating	7.4	7.1	6.3
Deteriorated coating or light slime	26.3	26.2	26.6
Heavy slime	45.6	45.9	47.8
Small calcareous fouling or weed	72.8	73.3	77.4
Medium calcareous fouling	107.1	108.2	118.3
Heavy calcareous fouling	157.1	158.2	163.9

The increase in the C_F values of the KCS due to a heavy slime condition at a ship speed of 24 knots was predicted to be ∼49%, ∼50% and ∼52%, by CFD-KCS hull, CFD-Flat plate and Granville's methods respectively, whereas these values altered to ∼163%, ∼164% and ∼171% respectively for a heavy calcareous fouling condition, as can be seen in Table 11 and Fig. 11.

The results presented in Table 12 and Fig. 12 indicate that the increase in C_F of the KCS due to heavy slime at a slow steaming ship speed of 19 knots was predicted to be ∼46%, ∼46% and ∼48%, by CFD-KCS hull, CFD-Flat plate and Granville's methods respectively, whereas these values altered to ∼157%, ∼158% and ∼164% respectively for a heavy calcareous fouling condition.

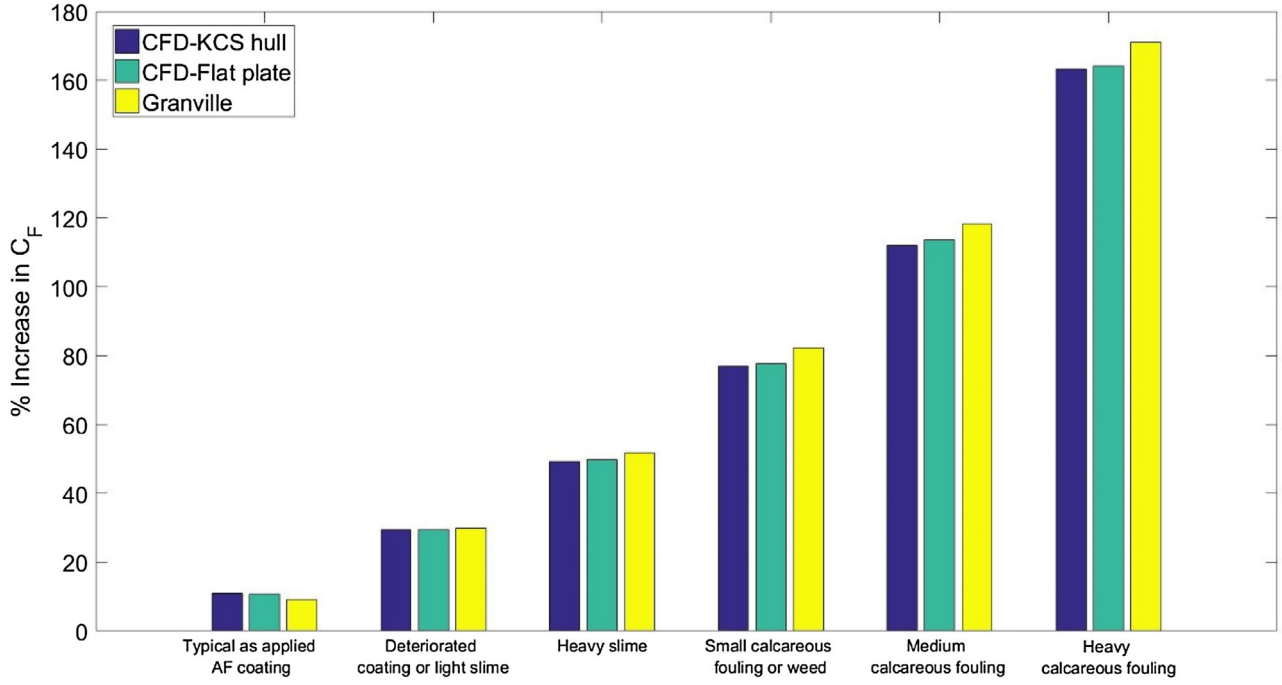

Fig. 11. Estimation of the percentage increase in the frictional resistance of the KCS due to different surface conditions at 24 knots ($Re = 2.89 \times 10^9$).

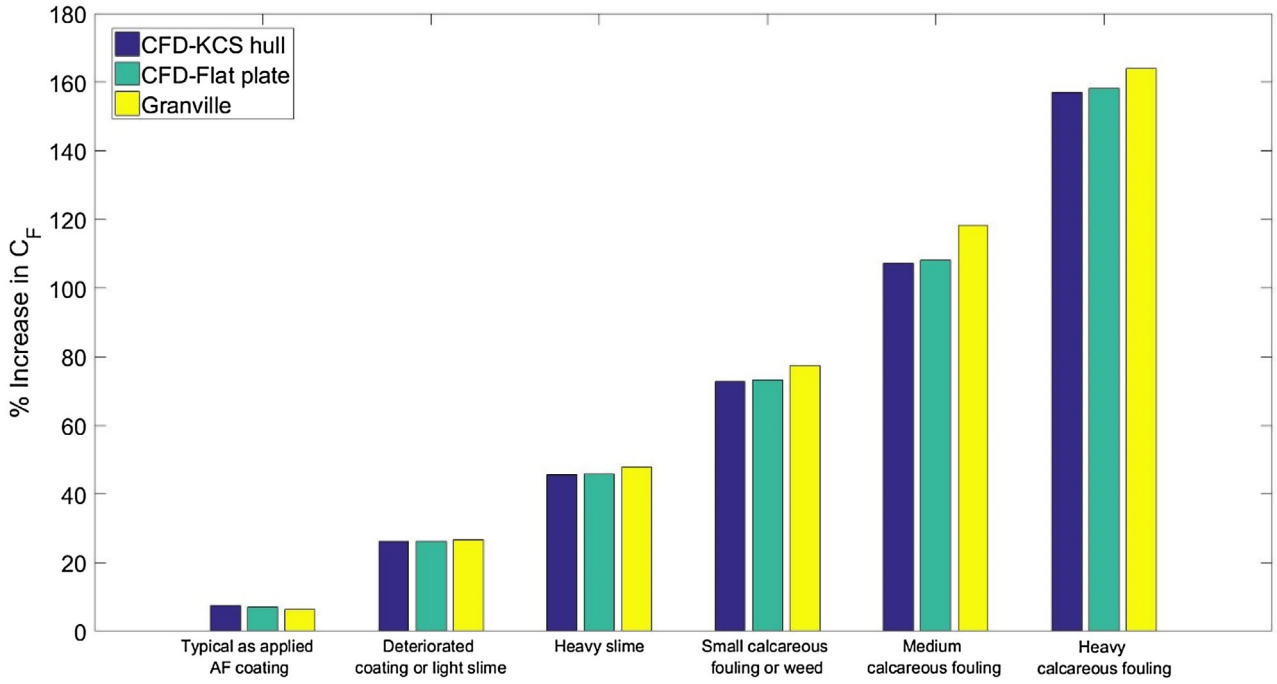

Fig. 12. Estimation of the percentage increase in the frictional resistance of the KCS due to different surface conditions at 19 knots ($Re = 2.29 \times 10^9$).

The results obtained using "CFD-KCS hull" method presented in Tables 11 and 12 indicate that the increase in C_F due to the hull roughness of a typical antifouling (AF) coating is 10.9% at 24 knots and 7.4% at 19 knots, whereas the increase in C_F due to biofouling is predicted to be dramatic, which would lead to a drastic increase in the fuel consumption and hence CO_2 emissions. The increase in the frictional resistance of the KCS due to a deteriorated coating or light slime surface condition was predicted to be 29.4% at a ship speed of 24 knots and to be 26.3% at a ship speed of 19 knots. These values became 49.2% and 45.6% when calculating the increase in C_F due to a heavy slime condition. Calcareous fouling causes significant increase in C_F values, ranging from ~77% to ~163% at 24 knots and ~73% to ~157% at 19 knots, depending on the type of calcareous fouling and ship speed.

The results presented are in accordance with the results of Schultz [15]. It should be borne in mind that the increase due to roughness of different marine coatings are still of importance when considering the fuel consumption of a ship.

4.4.2. *Residuary and wave resistance*

Residuary resistance coefficient, C_R, values of the full-scale KCS model were directly predicted by the present CFD simulations.

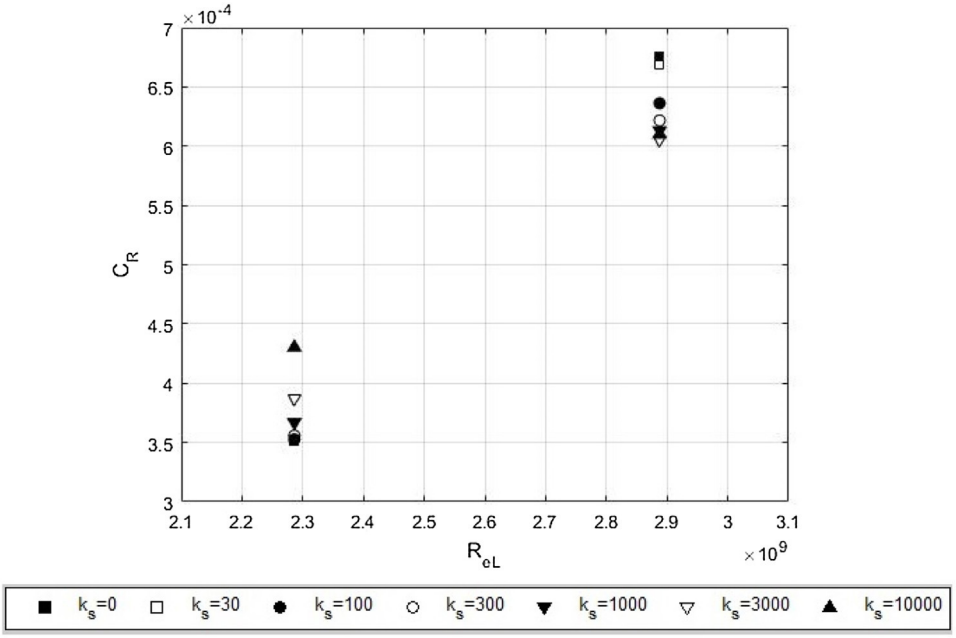

Fig. 13. C_R values of the full scale KCS for different surface conditions at ship speeds of 19 ($Re = 2.29 \times 109$) and 24 knots ($Re = 2.89 \times 10^9$).

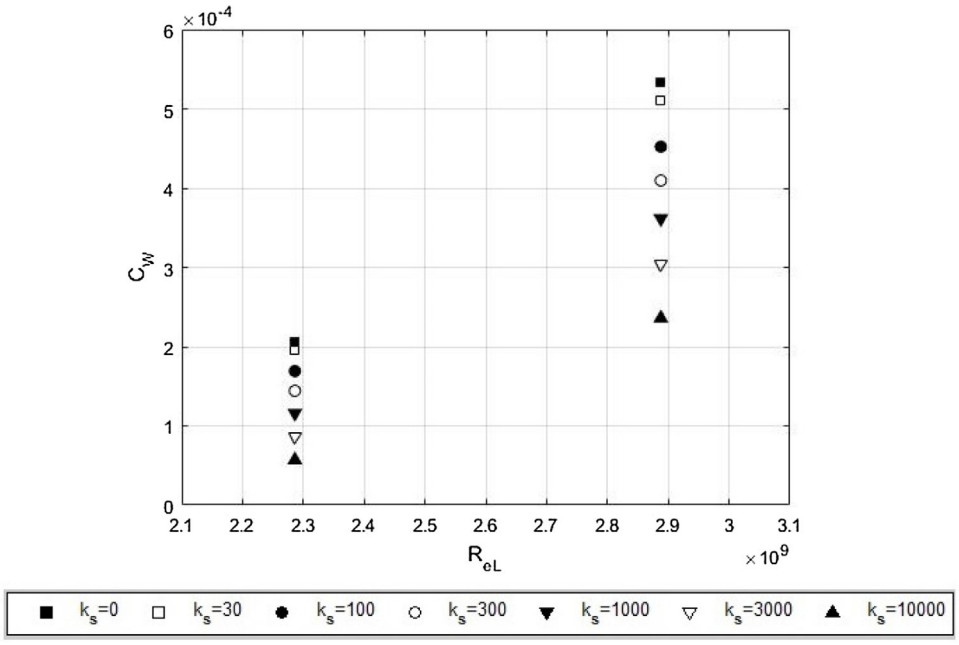

Fig. 14. C_W values of the full scale KCS for different surface conditions at ship speeds of 19 (Re = 2.29 × 109) and 24 knots (Re = 2.89 × 10^9).

Table 13
Computed% ΔC_W values at full scale at 24 knots (Re = 2.89 × 10^9) and at 19 knots (Re = 2.29 × 10^9).

Description of condition	24 knots	19 knots
Hydraulically smooth surface	–	–
Typical as applied AF coating	−4.4	−5
Deteriorated coating or light slime	−15.2	−17.9
Heavy slime	−23.2	−30.1
Small calcareous fouling or weed	−32.2	−43.8
Medium calcareous fouling	−43	−57.9
Heavy calcareous fouling	−55.8	−72.3

Fig. 13 shows the computed residuary resistance coefficients of the KCS hull obtained for 7 different surface conditions at ship speeds of 19 knots (Re = 2.29 × 10^9) and 24 knots (Re = 2.89 × 10^9).

Surprisingly, the residuary resistance coefficients showed an increasing trend with increasing fouling rates at 19 knots whereas it tended to decrease with increasing fouling rates at 24 knots. This is due to the fact that residuary resistance comprises viscous pressure resistance and wave resistance as shown by Eq. (14). These different trends can be attributed to the fact that the contribution of the viscous pressure resistance becomes more important than wave resistance at lower speeds. In other words, at higher speeds, the wave-making resistance becomes dominant due to wave generation.

Since viscous pressure resistance is a function of frictional resistance, it is appropriate to decompose the residuary resistance and investigate the effect of hull roughness on the wave resistance, R_W, using Eq. (15) and taking the form factor 1 + k = 1.1 [37]. Fig. 14 shows the calculated wave resistance coefficients, C_W, of the KCS hull obtained for 7 different surface conditions at ship speeds of 19 knots (Re = 2.29 × 10^9) and 24 knots (Re = 2.89 × 10^9).

As can be seen from Fig. 14, the wave resistance continuously decreased with increasing fouling rates. Table 13 and Fig. 15 demonstrate the change in the wave resistance of the KCS due to different surface conditions with respect to the smooth condition at a design speed of 24 knots and at a slow steaming speed of 19 knots, respectively.

The results presented in Table 13 and Fig. 15 indicate that the reduction in the C_W of the KCS due to a typical, as applied AF coating were predicted to be 4.4% and 5% whereas those due to a deteriorated coating or light slime were computed to be 15.2% and 17.9% at ship speeds of 24 knots and 19 knots, respectively. It was shown that the effect of heavy slime on the KCS hull caused a reduction in the C_W of 23.2% at 24 knots and 30.1% at 19 knots. The calcareous fouling would decrease C_W by up to 55.8% at 24 knots and 72.3% at 19 knots. An interesting point to note is that the effect of a particular fouling condition on the wave resistance of the KCS is more dominant at lower speeds. This can be attributed to the fact that the contribution of the viscous effects becomes more important at lower speeds.

Fig. 16 compares the global wave patterns around the hull surface of the KCS in smooth and heavy calcareous fouling conditions at 24 knots, while Fig. 17 shows the wave profile along a line with constant y = 0.1509.

It is seen from the comparison in Figs. 16 and 17 that wave amplitudes appear to be reduced by roughness effects. This is an indication of the effect of viscosity on the wave systems. The resulting free surface elevation around the KCS hull was recorded to range from −1.406 m to 3.357 m for smooth condition, and −1.345 m to 2.266 for heavy calcareous fouling condition (Fig. 16). This reduction of the wave system is in agreement with the computed reduction in wave resistance coefficients shown in Figs. 14 and 15 and Table 13.

As can be seen from Fig. 17 that the bow wave profiles computed for the smooth and heavy calcareous fouling conditions are on top of each other whereas the wave profiles deviate from each other in the wake region. This drastic reduction of the stern wave system and the obvious viscous effects on the wave resistance and wave systems is consistent with the findings of Raven, Van der Ploeg [56].

4.4.3. Total resistance and effective power

In order to reveal the effect of biofouling on the fuel consumption, the increase in the total resistance and hence the effective power of the KCS were calculated. An increase in the total resistance would increase the effective power, P_E, of a ship, which is the necessary power to move a ship through water. P_E is related to the total resistance, R_T, and ship speed, V, which is defined by Eq. (19).

$$P_E = R_T V \tag{19}$$

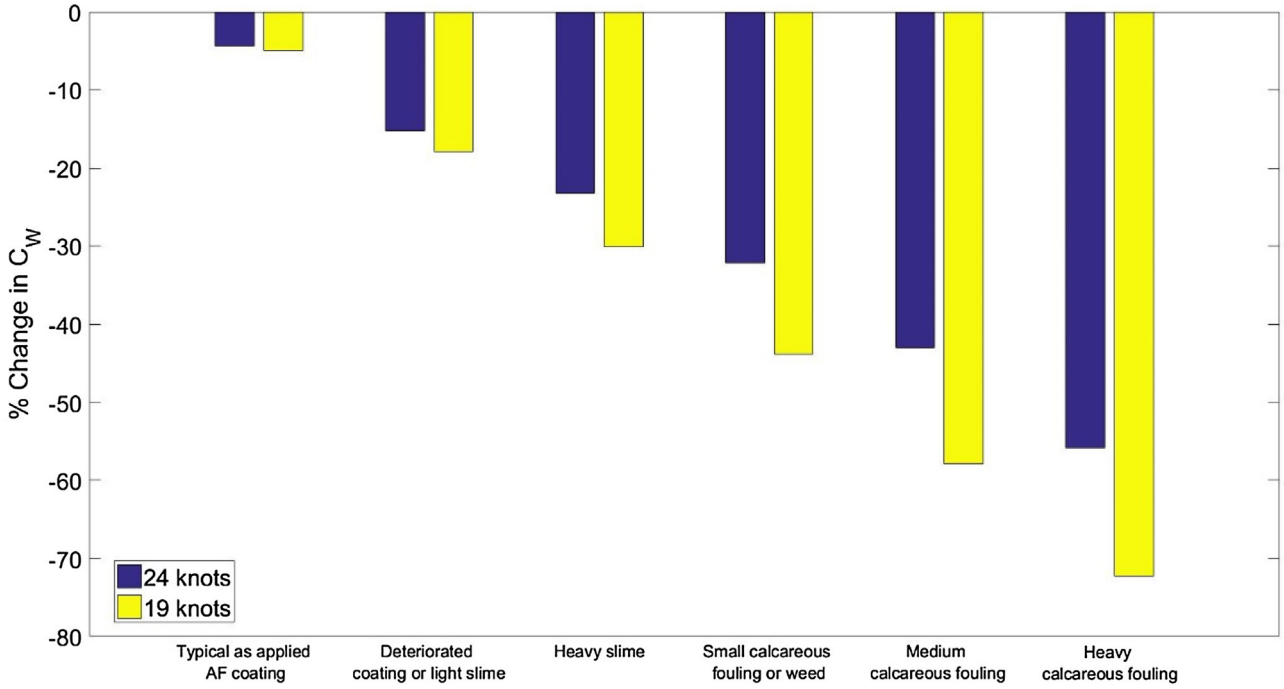

Fig. 15. Estimation of the percentage change in the wave resistance of the KCS due to different surface conditions at 24 knots ($Re = 2.89 \times 10^9$).

Table 14
Computed % ΔC_T, ΔP_E values at full scale at 24 knots ($Re = 2.89 \times 10^9$) and at 19 knots ($Re = 2.29 \times 10^9$).

Description of condition	24 knots	19 knots
Hydraulically smooth surface	–	–
Typical as applied AF coating	7.1	5.9
Deteriorated coating or light slime	18.1	21.2
Heavy slime	30.8	37.0
Small calcareous fouling or weed	49.1	59.5
Medium calcareous fouling	72.6	88.2
Heavy calcareous fouling	107.5	130.9

where

$$R_T = \frac{1}{2}\rho S C_T V^2 \tag{20}$$

where ρ is the density of water, S is the wetted surface area, C_T is the total resistance coefficient.

We can then re-write Eq. (19) as

$$P_E = \frac{1}{2}\rho S C_T V^3 \tag{21}$$

The increase in P_E due to the effect of fouling can be expressed by

$$\%\Delta P_E = \frac{C_{T,rough} - C_{T,smooth}}{C_{T,smooth}} \times 100 \tag{22}$$

similar to that used by Tezdogan et al. [49].

Total drag coefficient values of the full-scale KCS model were directly predicted by the present CFD simulations. Fig. 18 shows the predicted total resistance coefficients of the KCS hull obtained for 7 different surface conditions at ship speeds of 19 knots ($Re = 2.29 \times 10^9$) and 24 knots ($Re = 2.89 \times 10^9$).

As can be seen from Fig. 18, the effective power continuously increased with increasing fouling rates. Table 14 and Fig. 19 demonstrate the increase in the total resistance and hence in the effective power of the KCS due to different surface conditions with respect to the smooth condition at a design speed of 24 knots and at a slow steaming speed of 19 knots, respectively.

The results presented in Table 14 and Fig. 19 indicate that the increase in the C_T and P_E of the KCS due to a typical, as applied antifouling (AF) coating were predicted to be 7.1% and 5.9% whereas those due to a deteriorated coating or light slime may increase to 18.1% and 21.2% at ship speeds of 24 knots and 19 knots, respectively. The effect of heavy slime on the KCS hull was calculated to cause an increase in the C_T and P_E of 30.8% at 24 knots and 37% at 19 knots. The calcareous fouling would increase P_E by up to 107.5% at 24 knots and 130.9% at 19 knots.

An interesting point to note is that the effect of a particular fouling condition on the effective power of the KCS is more dominant at lower speeds. This can be attributed to the fact that the contribution of the frictional resistance becomes more important than residuary resistance at lower speeds. In other words, at higher speeds, the wave-making resistance becomes dominant due to wave generation. Therefore, the effect of a given fouling condition on the total resistance of a ship is greater at low to moderate speeds than at higher speeds [6].

4.4.4. *Velocity and turbulent kinetic energy distribution*

Velocity and turbulent kinetic energy contours in smooth and heavy calcareous fouling conditions are shown in Fig. 20 for the KCS ship hull and in Fig. 21 for the flat plate. Fig. 22 demonstrates cross sections of axial velocity contours at x/L = 0.25, 0.5, 0.75, depicting the boundary layer of the KCS hull in smooth and heavy calcareous fouling conditions.

As can be seen from Figs. 20–22, the turbulent kinetic energy increases with surface roughness whereas the velocity magnitude and axial velocity decreases with the existence of roughness on hull surface. It is in agreement with the fact that surface roughness leads to an increase in turbulence, which means that the turbulent stress and wall shear stress increase and ultimately, the velocity in the turbulent boundary layer decreases [57,58]. It should also be considered that the decrease in the velocity profile manifests itself as an increase in the frictional resistance [39]. As visually evident

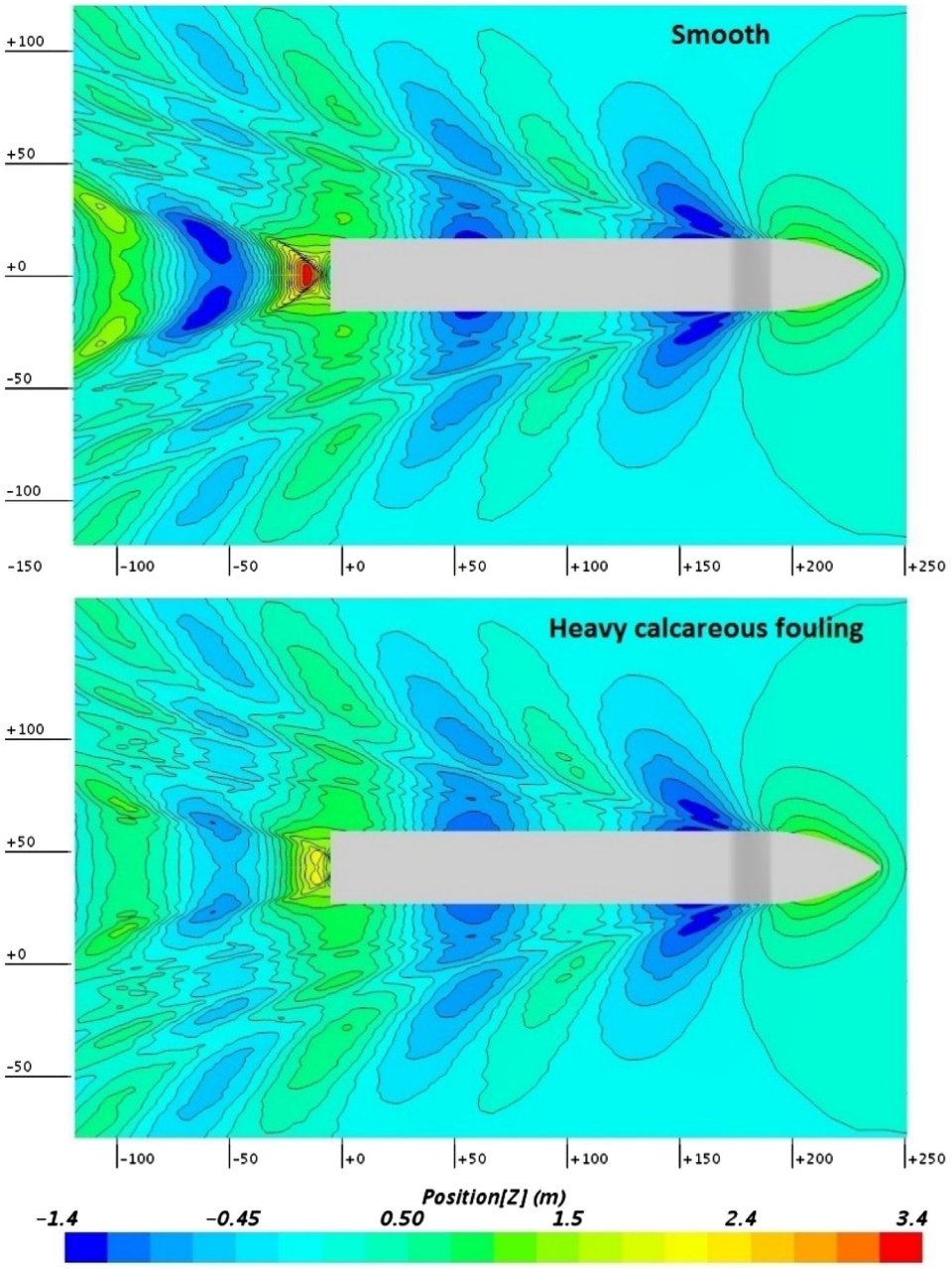

Fig. 16. Wave pattern around the KCS for smooth and heavy calcareous fouling conditions (V = 24 knots).

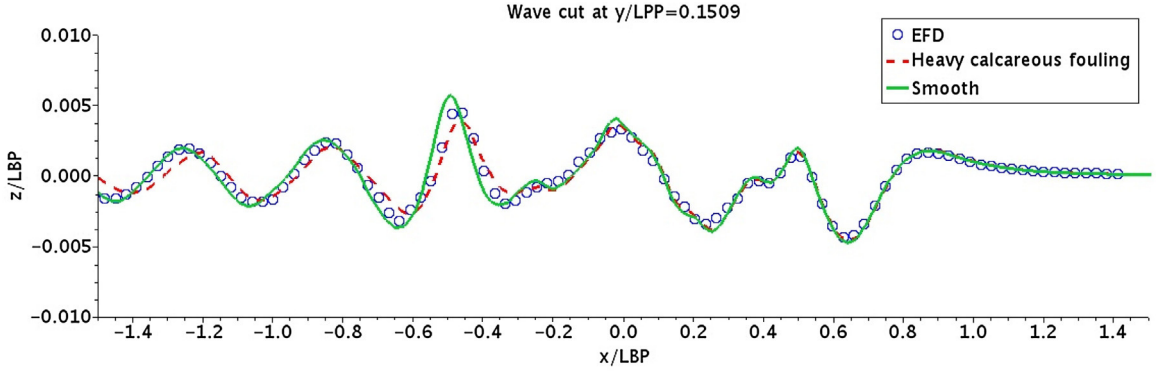

Fig. 17. Wave profiles at y = 0.1509 (V = 24 knots).

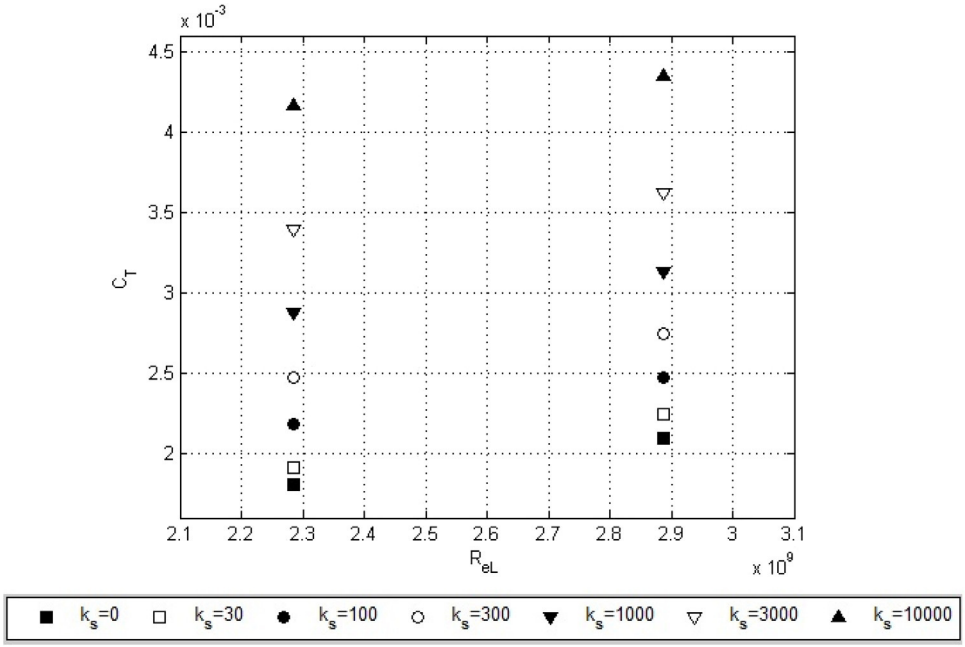

Fig. 18. C_T values of the full scale KCS for different surface conditions at ship speeds of 19 (Re = 2.29 × 109) and 24 knots (Re = 2.89 × 10^9).

from Fig. 22, the existence of heavy calcareous fouling on the KCS hull caused increases in the boundary layer thickness, δ, which is defined as the distance between the wall and the point where the axial velocity magnitude of the flow reaches the proportion of 0.99 of the free-stream velocity, i.e. U = 0.99 V, compared to an otherwise identical fouling-free KCS. The present findings are consistent with the experimental data of other researchers (e.g. Schultz and Flack [41], Schultz and Flack [59], Flack et al. [60], Flack et al. [61], Schultz [62]).

It is interesting to note that the velocity and turbulent kinetic energy contours shown in Figs. 20 and 22 are unexpectedly showing a spike at the centre plane due to the implementation of symmetry conditions at the symmetry plane (see Fig. 6).

5. Discussion and conclusions

A CFD model for the prediction of the effect of biofouling on ship resistance has been proposed and the effect of biofouling on ship resistance was investigated using CFD. A new roughness function model, which was developed based on the roughness function values of Schultz and Flack [41], was proposed and employed in the wall-function of the solver and a series of unsteady RANS simulations were carried out to predict the effect of a range of representative coating and biofouling conditions on the resistances of flat plates representing the KCS and the full-scale KCS model appended with a rudder. Firstly, the total resistance coefficient of the full-scale KCS model was obtained at a ship speed of 24 knots and compared

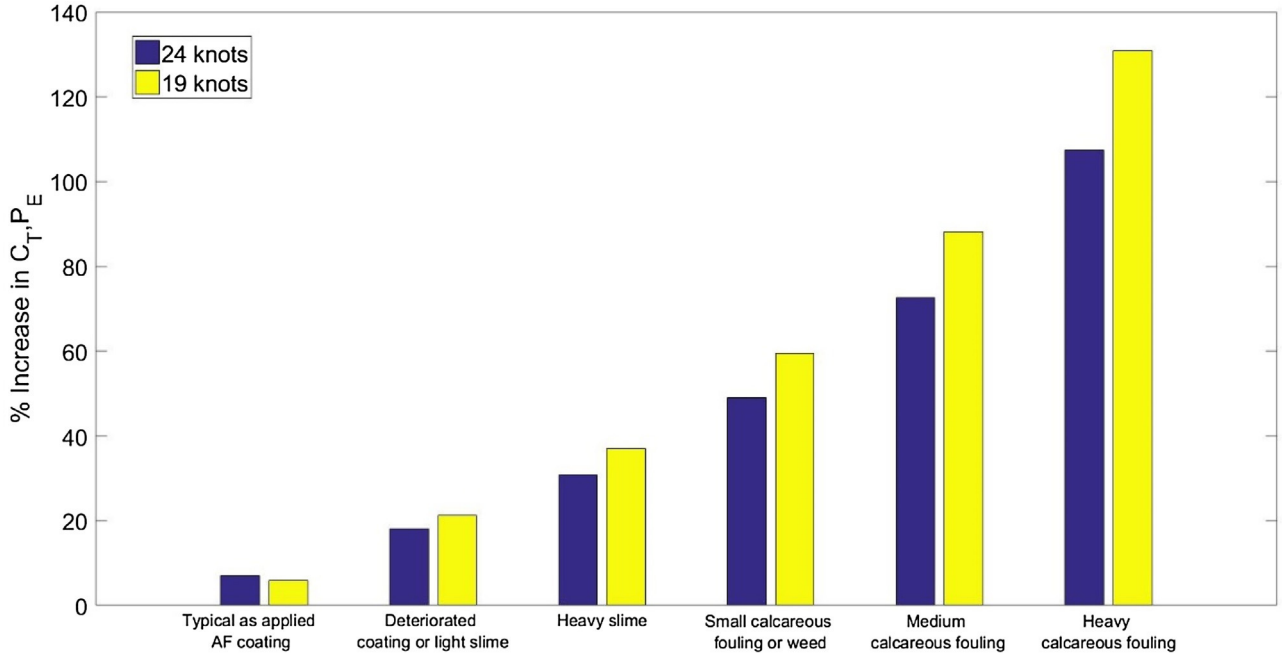

Fig. 19. Estimation of the percentage increase in the resistance and effective power of the KCS due to different surface conditions at 24 knots (Re = 2.89 × 10^9).

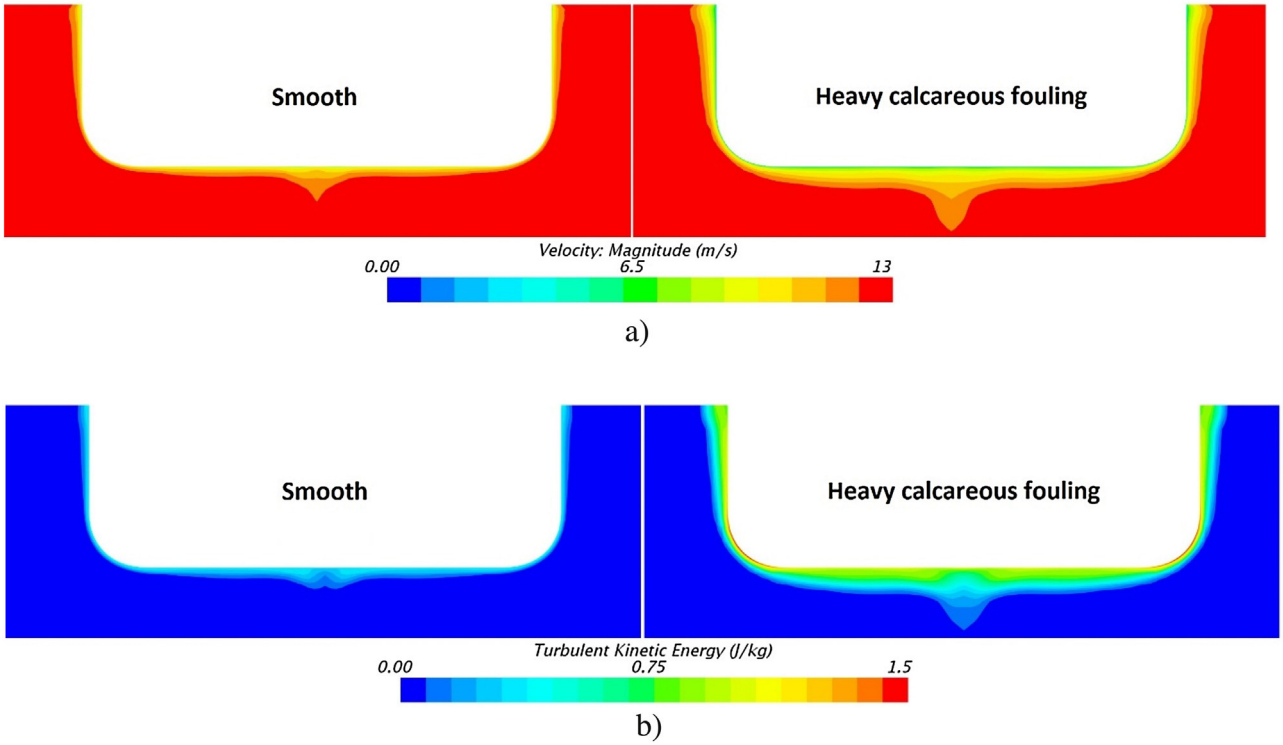

Fig. 20. a) Velocity and b) turbulent kinetic energy contours at the midship of the KCS hull for smooth and heavy calcareous fouling conditions (V = 24 knots).

with the total resistance coefficient extrapolated using the experimental data of Kim et al. [50] for validation. It was shown that the total resistance coefficient was over-predicted by 1.17% with a numerical uncertainty of ~0.74%. Following this, systematic studies were performed using the flat plates covered with heavy slime and using the KCS hull appended with a rudder with a smooth surface condition, in order to carry out a grid sensitivity study and to predict the CFD uncertainties.

Fully nonlinear unsteady RANS simulations to predict the effect of a range of representative coating and biofouling conditions on the frictional resistances of a flat plate, representing the KCS, and on the frictional, residuary, wave and total resistance and effective power of the KCS, have been carried out at two speeds, corresponding to service and slow steaming speeds.

The resulting C_F values obtained using flat plate CFD simulations and using 3D full-scale CFD simulations were compared with each other and with those obtained using the similarity law procedure of Granville [9] to examine the applicability of the proposed CFD model, since the literature does not offer any full-scale experimental results. It was shown that the present CFD model can be used for simulating roughness effects on the frictional resistance of flat plates and on the resistance of full-scale 3D ship hulls and that different types of roughness can be defined by modifying the wall-function of the software. This means that the CFD method can be used to predict the effects of such roughness on the resistance components of any arbitrary body without being obliged to conduct further experiments, once the relationship between the roughness functions and roughness Reynolds numbers of each surface is known.

The increase in the effective power of the full-scale KCS hull were predicted to be 7.1% at a ship speed of 24 knots and 5.9% at a ship speed of 19 knots for a typical as applied antifouling (AF) coating, 18.1% at 24 knots and 21.2% at 19 knots for a deteriorated coating or light slime condition and 30.8% at 24 knots and 37% at 19 knots for a heavy slime condition. These values altered to 49.1%, 72.6% and 107.5% at 24 knots and 59.5%, 88.2% and 130.9% at 19 knots for small calcareous fouling or weed, medium calcareous fouling and heavy calcareous fouling, respectively.

An important finding of the study is that the wave resistance and wave systems are significantly affected by the hull roughness and hence viscous effects, which is contrary to the major assumption which proposes that the wave resistance is not markedly affected by surface roughness and viscosity. The reduction in the wave resistance of the KCS hull in heavy calcareous fouling condition was found to be 55.8% at 24 knots and 72.3% at 19 knots.

It should be borne in mind that this study's aim was to propose a robust CFD model to predict the fouling impact on ship resistance. For this reason, an appropriate representative roughness function model was employed in spite of the slight discrepancies between the individual roughness function values and the model, especially in the transitionally rough regime. Without a doubt, these conditions and the roughness functions used in this paper may not necessarily represent all types of fouling conditions, since the assumptions made are based on the observations made in [6,15]. Future pieces of work may be the investigation of the roughness function behaviours of heterogeneous fouling accumulation, as seen on hulls, and an investigation into the range of applicability of the selected roughness length scale for the present conditions.

Having shown the applicability of the wall-function approach to account for the roughness effects of AF coatings and biofouling on full-scale 3D ship hulls, this approach can be used to simulate this effect on more complex structures such as on self-propelled ships with a rotating propeller. Another interesting future plan is to investigate the roughness effects on the total drag and effective power of ships of a more realistic spatial distribution of fouling on ship hulls.

It is important to note that the application of the proposed wall-functions does not cause any additional run-time for a typical CFD

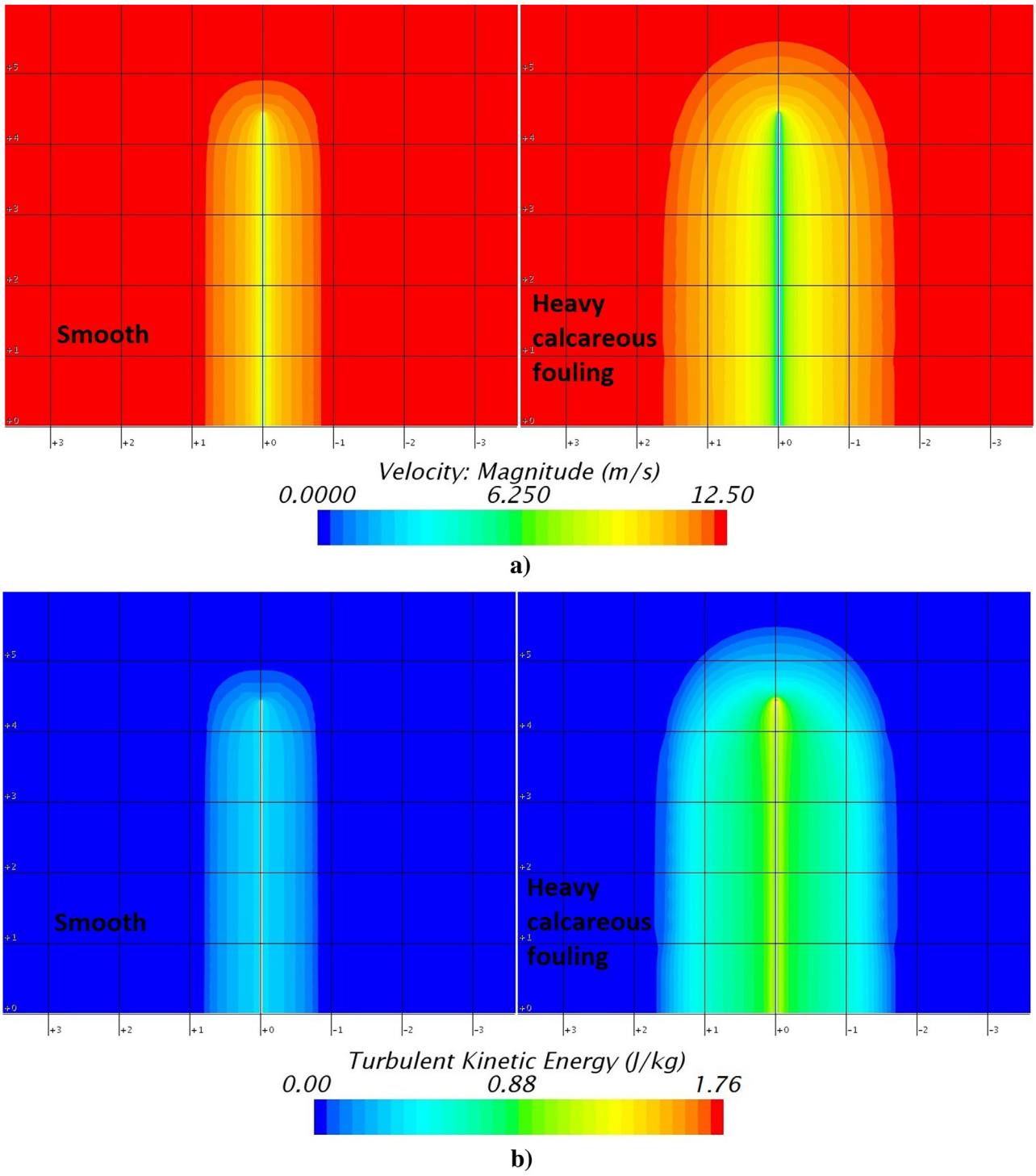

Fig. 21. a) Velocity and b) turbulent kinetic energy contours at the midship of the flat plate representing KCS hull for smooth and heavy calcareous fouling conditions (V = 24 knots) (Grid spacing is in meter).

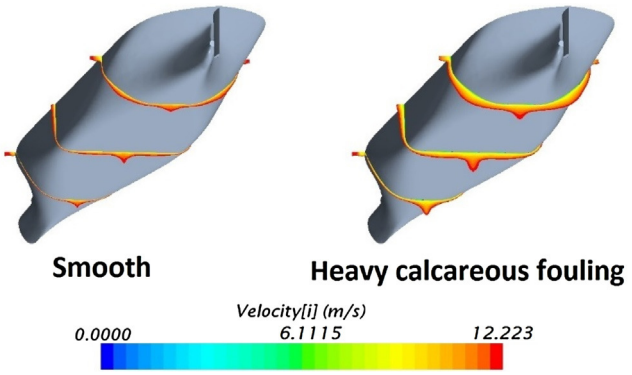

Fig. 22. Cross sections coloured with axial velocity limited to U = 0.99 V depicting the boundary layer (V = 24 knots).

simulation. That is to say, the run-time of CFD simulations of any arbitrary body with any surface roughness would be literally identical to those of CFD simulations of the same body with an otherwise smooth surface condition.

The main advantage of the proposed approach is that it enables the prediction of the effect of a typical coating and different biofouling conditions on the resistance of a ship under the effect of a rotating propeller or under the effect of a dynamic fluid-body interaction, which is not possible using the similarity law scaling procedure. Therefore, this approach stands as a practical prediction method for both academia and industry.

Acknowledgements

The authors are grateful for the EPSRC support for the project on 'Shipping in Changing Climates' (EPSRC Grant No. EP/K039253/1) which enabled them to carry out the research reported in this paper.

The authors gratefully acknowledge that the research presented in this paper was partially generated as part of the EU funded FP7 project FOUL-X-SPEL (Environmentally Friendly Antifouling Technology to Optimise the Energy Efficiency of Ships, Project number 285552, FP7-SST-2011-RTD-1).

It should be noted that the results were obtained using the EPSRC funded ARCHIE-WeSt High Performance Computer (www.archie-west.ac.uk). EPSRC grant no. EP/K000586/1. The underlying data in this paper is openly available from the University of Strathclyde data repository at: http://dx.doi.org/10.15129/adeb0db8-fec9-46ce-bbe3-9b828d0b9d35.

References

[1] IMO. Annex 5, Resolution MEPC. 245(66), 2014 Guidelines on the method of calculation of the attained Energy Efficiency Design Index (EEDI) for new ships. http://www.imo.org/KnowledgeCentre/IndexofIMOResolutions/MEPC%20Resolutions/MEPC%20245%2066.pdf, Marine Environment Protection Committee, 2014.
[2] IMO. Annex 9, Resolution MEPC.213(63), 2012 Guidelines for the development of a Ship Energy Efficiency Management Plan (SEEMP). http://www.imo.org/KnowledgeCentre/IndexofIMOResolutions/Documents/MEPC%20-%20Marine%20Environment%20Protection/213(63).pdf, Marine Environment Protection Committee, 2012.
[3] IMO. MEPC 59/4/15, Prevention of air pollution from ships, Energy Efficiency Operational Indicator (EEOI) http://www.rina.org.uk/hres/mepc%2059_4_16.pdf, Marine Environment Protection Committee, 2009.
[4] IMO. Second IMO GHG Study. 2009.
[5] RAEng. Future Ship Powering Options. 2013.
[6] M.P. Schultz, Effects of coating roughness and biofouling on ship resistance and powering, Biofouling 23 (2007) 331–341.
[7] T. Tezdogan, Y.K. Demirel, An overview of marine corrosion protection with a focus on cathodic protection and coatings, Brodogradnja 65 (2014) 49–59.
[8] ITTC. Specialist Committee on Surface Treatment–Final report and recommendations to the 26th ITTC. Proceedings of 26th ITTC–Volume II http://ittcinfo/media/5532/11pdf2011.
[9] P.S. Granville, The frictional resistance and turbulent boundary layer of rough surfaces, J. Ship Res. 2 (1958) 52–74.
[10] P.S. Granville, Similarity-law characterization methods for arbitrary hydrodynamic roughnesses, in: Final Report Naval Ship Research and Development Center, Ship Performance Dept., Bethesda, MD, 1978, pp. 1.
[11] G. Loeb, D. Laster, T. Gracik, The influence of microbial fouling films on hydrodynamic drag of rotating discs, in: J.D. Costlow, R. Tipper (Eds.), Marine Biodeterioration: An Interdisciplinary Study, Naval Institute Press, Annapolis, MD, 1984, pp. 88–94.
[12] E.G. Haslbeck, G. Bohlander, Microbial biofilm effects on drag-lab and field, in: Ship Production Symposium Proceedings, SNAME1992, 1992.
[13] M.P. Schultz, The Effect of Biofilms on Turbulent Boundary Layer Structure, Florida Institute of Technology, 1998.
[14] M.P. Schultz, The relationship between frictional resistance and roughness for surfaces smoothed by sanding, J. Fluids Eng. 124 (2002) 492–499.
[15] M.P. Schultz, Frictional resistance of antifouling coating systems, J. Fluids Eng. 126 (2004) 1039–1047.
[16] T.A. Shapiro, The effect of surface roughness on hydrodynamic drag and turbulence. USNA Trident Scholar Project Report No. 3272004.
[17] K.A. Flack, M.P. Schultz, Review of hydraulic roughness scales in the fully rough regime, J. Fluids Eng. 132 (2010) 041203.
[18] M.P. Schultz, J.A. Bendick, E.R. Holm, W.M. Hertel, Economic impact of biofouling on a naval surface ship, Biofouling 27 (2011) 87–98.
[19] J.M. Walker, M.P. Schultz, K.A. Flack, C.N. Steppe, Skin-friction drag measurements on ship hull coating systems, 30th Symposium on Naval Hydrodynamics (2015) 1–10.
[20] C. Grigson, The drag at ship scale of planes having any quality of roughness, J. Ship Res. 29 (1985) 94–104.
[21] G.H. Christoph, R.H. Pletcher, Prediction of rough-wall skin friction and heat transfer, AIAA J. 21 (1983) 509–515.
[22] D. Lakehal, Computation of turbulent shear flows over rough-walled circular cylinders, J. Wind Eng. Ind. Aerodyn. 80 (1999) 47–68.
[23] G. Greígoire, M. Favre-Marinet, F.J.S. Amand, Modeling of turbulent fluid flow over a rough wall with or without suction, J. Fluids Eng. 125 (2003) 636–642.
[24] V.C. Patel, Perspective: flow at high reynolds number and over rough surfaces—Achilles heel of CFD, J. Fluids Eng. 120 (1998) 434–444.
[25] K. Suga, T.J. Craft, H. Iacovides, An analytical wall-function for turbulent flows and heat transfer over rough walls, Int. J. Heat Fluid Flow 27 (2006) 852–866.
[26] D. Apsley, CFD calculation of turbulent flow with arbitrary wall roughness, Flow Turbul. Combust. 78 (2007) 153–175.
[27] P.-A. Krogstad, Modification of the van Driest damping function to include the effects of surface roughness, AIAA J. 29 (1991) 888–894.
[28] B. Aupoix, A general strategy to extend turbulence models to rough surfaces: application to Smith's k-L model, J. Fluids Eng. 129 (2007) 1245–1254.
[29] L. Eça, M. Hoekstra, Numerical aspects of including wall roughness effects in the SST k–(eddy-viscosity turbulence model, Comput. Fluids 40 (2011) 299–314.
[30] J.C. Date, S.R. Turnock, A Study into the Techniques Needed to Accurately Predict Skin Friction Using RANS Solvers with Validation Against Froude's Historical Flat Plate Experimental Data, University of Southampton, Southampton, UK, 1999, 62pp.
[31] M. Leer-Andersen, L. Larsson, An experimental/numerical approach for evaluating skin friction on full-scale ships with surface roughness, J. Mar. Sci. Technol. 8 (2003) 26–36.
[32] P. Izaguirre-Alza, L. Pérez-Rojas, J.F. Núñez-Basáñez, Drag reduction through special paints coated on the hull, in: International Conference on Ship Drag Reduction SMOOTH-SHIPS, Istanbul, Turkey, 2010.
[33] Y.S. Khor, Q. Xiao, CFD simulations of the effects of fouling and antifouling, Ocean Eng. 38 (2011) 1065–1079.
[34] T. Cebeci, P. Bradshaw, Momentum Transfer in Boundary Layers, Hemisphere Publishing Corporation, McGraw-Hill, 1977.
[35] J. Nikuradse, Laws of flow in rough pipes: NACA Technical Memorandum 1292, 1933.
[36] ITTC, Practical Guidelines for Ship CFD Application. ITTC Recommended Procedures and Guidelines, Procedure 75-03-02-03, Revision 012011.
[37] A.M. Castro, P.M. Carrica, F. Stern, Full scale self-propulsion computations using discretized propeller for the KRISO container ship KCS, Comput. Fluids 51 (2011) 35–47.
[38] ITTC. Report of the Powering Performance Committee. Proceedings of the 19th ITTC. http://ittc.info/media/2304/report-of-the-power-performance-committee.pdf1990.
[39] Y.K. Demirel, M. Khorasanchi, O. Turan, A. Incecik, M.P. Schultz, A CFD model for the frictional resistance prediction of antifouling coatings, Ocean Eng. 89 (2014) 21–31.
[40] M. Haase, K. Zurcher, G. Davidson, J.R. Binns, G. Thomas, N. Bose, Novel CFD-based full-scale resistance prediction for large medium-speed catamarans, Ocean Eng. 111 (2016) 198–208.
[41] M.P. Schultz, K. Flack, The rough-wall turbulent boundary layer from the hydraulically smooth to the fully rough regime, J. Fluid Mech. 580 (2007) 381–405.
[42] J. Jiménez, Turbulent flows over rough walls, Ann. Rev. Fluid Mechan. 36 (2004) 173–196.
[43] M.A. Shockling, J.J. Allen, A.J. Smits, Roughness effects in turbulent pipe flow, J. Fluid Mech. 564 (2006) 267–285.
[44] Naval Ships' Technical Manual. Waterborne underwater hull cleaning of navy ships. S9086-CQ-STM-010/CH-081R5. Naval Sea Systems Command. 2002.

[45] L. Hundley, Tate C. Hull-fouling studies and ship powering trial results on seven FF 1052 class ships. D W Taylor Naval Ship Research and Development Center Report # DTNSRDC-80/027 111 p. 1980.
[46] L. Larsson, F. Stern, V. Bertram, Benchmarking of computational fluid dynamics for ship flows: the Gothenburg 2000 workshop, J. Ship Res. 47 (2003) 63–81.
[47] Z-r. Zhang, Verification and validation for RANS simulation of KCS container ship without/with propeller, J. Hydrodyn. (Ser. B) (2010) 932–939.
[48] P.M. Carrica, H. Fu, F. Stern, Computations of self-propulsion free to sink and trim and of motions in head waves of the KRISO Container Ship (KCS) model, Appl. Ocean Res. 33 (2011) 309–320.
[49] T. Tezdogan, Y.K. Demirel, P. Kellett, M. Khorasanchi, A. Incecik, O. Turan, Full-scale unsteady RANS CFD simulations of ship behaviour and performance in head seas due to slow steaming, Ocean Eng. 97 (2015) 186–206.
[50] W.J. Kim, S.H. Van, D.H. Kim, Measurement of flows around modern commercial ship models, Exp. Fluids 31 (2001) 567–578.
[51] CD-ADAPCO. User Guide STAR-CCM+, Version 9.02.011. 2014.
[52] L.F. Richardson, The approximate arithmetical solution by finite differences of physical problems involving differential equations, with an application to the stresses in a masonry dam, Trans. R. Soc. Lond. 210 (1910) 307–357.
[53] L.F. Richardson, J.A. Gaunt, The deferred approach to the limit, Philos. Trans. R. Soc. Lond. 226 (1927) 299–361.
[54] I.B. Celik, U. Ghia, P.J. Roache, C.J. Freitas, H. Coleman, P.E. Raad, Procedure for estimation and reporting of uncertainty due to discretization in CFD applications, J. Fluids Eng. Trans. ASME 130 (2008), 078001-1-4.
[55] P.M. Carrica, A.M. Castro, F. Stern, Self-propulsion computations using a speed controller and a discretized propeller with dynamic overset grids, J. Mar. Sci. Technol. 15 (2010) 316–330.
[56] H.C. Raven, A. Van der Ploeg, A.R. Starke, L. Eça, Towards a CFD-based prediction of ship performance—progress in predicting full-scale resistance and scale effects, in: Proceedings of RINA Marine CFD Conference, London, UK, 2008.
[57] M.P. Schultz, G.W. Swain, The influence of biofilms on skin friction drag, Biofouling 15 (2000) 129–139.
[58] Y.K. Demirel, Modelling the Roughness Effects of Marine Coatings and Biofouling on Ship Frictional Resistance, University of Strathclyde, 2015 (PhD Thesis).
[59] M.P. Schultz, K.A. Flack, Outer layer similarity in fully rough turbulent boundary layers, Exp. Fluids 38 (2005) 328–340.
[60] K.A. Flack, M.P. Schultz, T.A. Shapiro, Experimental support for Townsend's Reynolds number similarity hypothesis on rough walls, Phys. Fluids 17 (2005) (1994-present).
[61] K.A. Flack, M.P. Schultz, Connelly JS: Examination of a critical roughness height for outer layer similarity, Phys. Fluids 19 (2007) 095104.
[62] M.P. Schultz, Turbulent boundary layers on surfaces covered with filamentous algae, J. Fluids Eng. 122 (2000) 357–363.